

Theory of spin blockade, charge ratchet effect, and thermoelectrical behavior in serially coupled quantum-dot system

David M.-T. Kuo^{1†}, Shiue-Yuan Shiao², and Yia-chung Chang^{2*}

¹*Department of Electrical Engineering and Department of Physics,
National Central University, Chungli, 320 Taiwan and*

²*Research Center for Applied Sciences, Academic Sinica, Taipei, 11529 Taiwan*

(Dated: September 2, 2018)

The charge transport of a serially coupled quantum dots (SCQD) connected to the metallic electrodes is theoretically investigated in the Coulomb blockade regime. A closed-form expression for the tunneling current of SCQD in the **weak interdot hopping** limit is obtained by solving an extended two-site Hubbard model via the Green's function method. We use this expression to investigate spin current rectification, negative differential conductance, and coherent tunneling in the nonlinear response regime. The current rectification arising from the space symmetry breaking of SCQD is suppressed by increasing temperature. The calculation of SCQD is extended to the case of multiple parallel SCQDs for studying the charge ratchet effect and SCQD with multiple levels. In the linear response regime, the functionalities of spin filter and low-temperature current filter are demonstrated to coexist in this system. It is further demonstrated that two-electron spin singlet and triplet states can be readily resolved from the measurement of Seebeck coefficient rather than that of electrical conductance.

I. INTRODUCTION

Tunneling current through individual quantum dots (QDs) with discrete levels exhibits a kaleidoscope of interesting physics such as the Kondo effect, Fano resonance, and Coulomb blockade.¹ Recently, a serially coupled quantum-dot (SCQD) system (the simplest artificial molecule) was proposed as a spin filter based on the spin-blockade process for **application in** spintronics and quantum computing.²⁻⁴ The transport properties of the SCQD in the Coulomb blockade regime include current rectification,²⁻⁴ negative differential conductance (NDC),²⁻⁴ nonthermal broadening of electrical conductance,^{5,6} and coherent tunneling for the SCQD with degenerate energy levels (quantum dot “helium”).⁶ Many theoretical efforts have been devoted to studying them.⁷⁻¹⁸ Nevertheless, there still **lacks** a comprehensive theory to explain these phenomena in a systematic way.¹⁹ The early studies of SCQD focused on the coherent transport behavior without spin dependence.^{9,10} For the application of spintronics and experimental observations of spin-dependent tunneling current, the current rectification arising **from** the Pauli spin blockade and NDC were theoretically studied by several groups.¹¹⁻¹⁴ The transport properties of SCQD embedded in a matrix connected **to** ferromagnetic electrodes were also studied.¹⁵⁻¹⁸ However, theoretical study of the nonthermal broadening of electrical conductance of SCQD in the presence of electron Coulomb interactions has not been reported.

Using the Green's function (GF) technique we have solved an extended Hubbard model, which includes the interdot Coulomb interactions as well as intradot Coulomb interactions for a coupled quantum dot system, in the weak interdot hopping strength limit. The derived closed-form solution for the transmission factor has eight spin-charge configurations and 16 resonant chan-

nels. With this theory we can provide quantitative analysis for current rectification arising from coherent tunneling with spin blockade, NDC, and nonthermal broadening effect of tunneling current resulting from the off-resonant energy levels. All our predictions are in good agreement with available experimental data.²⁻⁶ In addition, we demonstrate that the SCQD junction system can be used as a low-temperature current filter and spin filter simultaneously.

To depict the charge ratchet effect arising from other QDs surrounding the SCQD²⁰ and the case of SCQD with multiple levels (such as the Si-based SCQD, where the multi-valleyed nature of Si gives rise to closely-spaced energy levels in each Si QD,^{21,22} we extend our calculation to a four-level Anderson model by using a simple and physical picture. Unlike GaAs QD system with large **nuclear and electron spin** interactions,² Si QDs have longer electron spin coherent time, which is **an** important consideration for **quantum computing**. Owing to traps and impurities of Si QDs and **their** multi-valleyed characteristics^{21,22}, we need to consider **a** Hamiltonian beyond the two-level Anderson model. **However**, based on the conventional theoretical framework,¹ it is complicated to deal with carrier transport properties of multiple QDs. **In this paper, we propose a new and comparatively easy approach, which allows us to** derive a closed form solution of tunneling current for arbitrary QD numbers in the limit of **weak interdot hopping** strength. Based on this closed-form expression of tunneling current, we can fully analyze the tunneling current spectrum of multiple-SCQD system.

Recently, many theoretical efforts have been devoted to the studies of thermoelectric properties of QDs **in quest of** highly efficient thermoelectrical materials.²³⁻²⁷ However, these studies have focused **only** on the thermoelectrical properties of a single QD^{23,26} or parallel QDs.^{24,27} To reduce the temperature gradient across the QD junction,

it is essential to study the case of N coupled QDs in serial. In this paper, we also investigate the thermoelectric effect of SCQD. We find that the Seebeck coefficient is much larger in the spatially symmetric SCQD than the spatially asymmetric SCQD. Furthermore, we find that the measurement of Seebeck coefficient provides an alternative means to distinguish the spin singlet and triplet states in the linear response regime.

II. FORMALISM

The inset of Fig. 1 illustrates the model system of concern, showing a serially coupled quantum dots connected to metallic electrodes. The electron Hamiltonian can be described by a two-level Anderson model:⁸

$$\begin{aligned}
H = & \sum_{\mathbf{k},\sigma} \epsilon_{\mathbf{k}} a_{\mathbf{k},\sigma}^\dagger a_{\mathbf{k},\sigma} + \sum_{\mathbf{k},\sigma} \epsilon_{\mathbf{k}} b_{\mathbf{k},\sigma}^\dagger b_{\mathbf{k},\sigma} + \sum_{\ell,\sigma} E_{\ell,\sigma} d_{\ell,\sigma}^\dagger d_{\ell,\sigma} \\
& + \sum_{\ell} U_{\ell} d_{\ell,\uparrow}^\dagger d_{\ell,\uparrow} d_{\ell,\downarrow}^\dagger d_{\ell,\downarrow} + \frac{1}{2} \sum_{\ell \neq j; \sigma, \sigma'} U_{\ell,j} d_{\ell,\sigma}^\dagger d_{\ell,\sigma} d_{j,\sigma'}^\dagger d_{j,\sigma'} \\
& + \sum_{\mathbf{k},\sigma} [V_{\mathbf{k},A} a_{\mathbf{k},\sigma}^\dagger d_{A,\sigma} + V_{\mathbf{k},B} d_{B,\sigma}^\dagger b_{\mathbf{k},\sigma}] + h.c. \\
& + \sum_{\sigma} t_{12} (d_{A,\sigma}^\dagger d_{B,\sigma} + d_{B,\sigma}^\dagger d_{A,\sigma}), \quad (1)
\end{aligned}$$

where the first two terms describe, respectively, the free electron gas of the left and right metallic electrodes. The operators in the system Hamiltonian are defined as: $a_{\mathbf{k},\sigma}^\dagger$ ($a_{\mathbf{k},\sigma}$) creates (destroys) an electron of momentum \mathbf{k} and spin σ with energy $\epsilon_{\mathbf{k}}$ in the left metallic electrode. $b_{\mathbf{k},\sigma}^\dagger$ ($b_{\mathbf{k},\sigma}$) creates (destroys) an electron in the right electrode. $d_{\ell,\sigma}^\dagger$ ($d_{\ell,\sigma}$) creates (destroys) an electron in the ℓ th dot (dot A or dot B). U_{ℓ} and $U_{\ell,j}$ describe the Coulomb interactions inside the ℓ th dot and between the ℓ th and j th dots, respectively. For small semiconductor QDs (with size \sim nm), the orbital energy level separation of individual QD is much larger than U_{ℓ} and thermal energy $k_B T$. This allows us to consider only one energy level for each dot in Eq. (1). $V_{\mathbf{k},A(B)}$ describes the coupling between the band states of electrodes and **state** of dot A (B) with energy level E_1 (E_2). The last two terms describe the electron hopping between two dots.

Using the Keldysh-Green's function technique,^{1,2} we obtain the tunneling current expression of SCQD (see Appendix) as

$$J = \frac{2e}{h} \int d\epsilon \mathcal{T}(\epsilon) [f_L(\epsilon) - f_R(\epsilon)], \quad (2)$$

where $\mathcal{T}(\epsilon) \equiv \Gamma_L(\epsilon)\Gamma_R(\epsilon)(\mathcal{A}_{12} + \mathcal{A}_{21})/2$ is the transmission factor. $\Gamma_{\ell=L,R}(\epsilon)$ denote the tunnel **rates** from the left electrode to dot A and **from** the right electrode to dot B, **respectively**. $f_{L(R)}(\epsilon) = 1/[e^{(\epsilon - \mu_{L(R)})/k_B T_{L(R)}} + 1]$ denotes the Fermi distribution function for the left (right) electrode. The chemical potential difference between these two electrodes is related to $\mu_L - \mu_R = e\Delta V_a$. $T_{L(R)}$ denotes the equilibrium temperature of the left (right)

electrode. e and h denote the electron charge and Plank's constant, respectively. For simplicity, we consider the **wide-band limit**: $\Gamma_{\ell}(\epsilon) = \Gamma_{\ell}$. The "resonant function" $\mathcal{A}_{\ell,j}$ of the transmission factor can be calculated by the on-site retarded Green's function ($G_{\ell,\ell}^r(\epsilon)$) and the lesser Green's function ($G_{\ell,\ell}^<(\epsilon)$) (see Appendix).

After straightforward algebra, we obtain an expression for the resonant function

$$\mathcal{A}_{\ell,j}(\epsilon) = t_{12}^2 \sum_{m=1}^8 p_m / |\Pi_m|^2; \quad (\ell \neq j), \quad (3)$$

where the denominators for the eight configurations are: (i) $\Pi_1 = \mu_{\ell}\mu_j - t_{12}^2$ with both dots empty, (ii) $\Pi_2 = (\mu_{\ell} - U_{\ell,j})(\mu_j - U_j) - t_{12}^2$, with dot ℓ empty and dot j filled by one electron with spin $\bar{\sigma}$, (iii) $\Pi_3 = (\mu_{\ell} - U_{\ell,j})(\mu_j - U_{j,\ell}) - t_{12}^2$ with dot ℓ empty and dot j filled by one electron with spin σ , (iv) $\Pi_4 = (\mu_{\ell} - 2U_{\ell,j})(\mu_j - U_j - U_{j,\ell}) - t_{12}^2$ with dot ℓ is empty and dot j filled by two electrons, (v) $\Pi_5 = (\mu_{\ell} - U_{\ell})(\mu_j - U_{j,\ell}) - t_{12}^2$ with dot j empty and dot ℓ filled by one electron with spin $\bar{\sigma}$, (vi) $\Pi_6 = (\mu_{\ell} - U_{\ell} - U_{\ell,j})(\mu_j - U_j - U_{j,\ell}) - t_{12}^2$ with both dots filled by one electron with spin $\bar{\sigma}$, (vii) $\Pi_7 = (\mu_{\ell} - U_{\ell} - U_{\ell,j})(\mu_j - 2U_{j,\ell}) - t_{12}^2$ with dot ℓ filled by one electron with spin $\bar{\sigma}$ and dot j filled by one electron with spin σ , and (viii) $\Pi_8 = (\mu_{\ell} - U_{\ell} - 2U_{\ell,j})(\mu_j - U_j - 2U_{j,\ell}) - t_{12}^2$ with dot ℓ filled by one electron with spin $\bar{\sigma}$ and dot j filled by two electrons. $\mu_{\ell} = \epsilon - E_{\ell} + i\Gamma_{\ell}/2$. The numerators p_m 's denote the probability factors for various sin-charge configurations. They are $p_1 = (1 - N_{\ell,\bar{\sigma}})(1 - N_{j,\sigma} - N_{j,\bar{\sigma}} + c_j)$, $p_2 = (1 - N_{\ell,\bar{\sigma}})(N_{j,\bar{\sigma}} - c_j)$, $p_3 = (1 - N_{\ell,\bar{\sigma}})(N_{j,\sigma} - c_j)$, $p_4 = (1 - N_{\ell,\bar{\sigma}})c_j$, $p_5 = N_{\ell,\bar{\sigma}}(1 - N_{j,\sigma} - N_{j,\bar{\sigma}} + c_j)$, $p_6 = N_{\ell,\bar{\sigma}}(N_{j,\bar{\sigma}} - c_j)$, $p_7 = N_{\ell,\bar{\sigma}}(N_{j,\sigma} - c_j)$, and $p_8 = N_{\ell,\bar{\sigma}}c_j$ ($\bar{\sigma}$ denotes the opposite of σ), where $N_{\ell,\sigma}$ and c_{ℓ} denote the thermally averaged one-particle occupation number and two-particle correlation function, respectively. They can be obtained by

$$N_{\ell,\sigma} = \langle n_{\ell,\sigma} \rangle = \int \frac{d\epsilon}{2\pi} G_{\ell,\ell}^<(\epsilon), \quad (4)$$

$$c_{\ell} = \int \frac{d\epsilon}{2\pi} G_{\ell,\ell}^{2,<}(\epsilon), \quad (5)$$

where $G_{\ell,\ell}^<(\epsilon)$ and $G_{\ell,\ell}^{2,<}(\epsilon)$ denote, respectively, the on-site one-particle and two-particle lesser Green's functions, which can be calculated by the equation-of-motion method.

The expression of Eq. (3) is valid in the Coulomb blockade regime, but not in the Kondo regime, because we did not take into account the effect of electron Coulomb interaction on the tunneling rate (Γ_{ℓ}) which arises from the coupling between the electrodes and the QD. Eq. (3), also valid in the limit of $t_{12}/U \ll 1$, is correct up to the second order in t_{12} . This is sufficient for our analysis of weakly coupled dot, since in the SCQD system the value of hopping strength t_{12} is much smaller than all the other energy scales. When $t_{12}/\Gamma_{\ell} \ll 1$, we can safely neglect in the lesser Green's functions the corrections coming from the neighboring dot. Eqs. (4) and

(5) can then be rewritten in terms of the on-site retarded Green's functions: $N_{\ell,\sigma} = -(1/\pi) \int d\epsilon f_{\ell}(\epsilon) \text{Im}G_{\ell,\ell}^r(\epsilon)$, and $c_{\ell} = -(1/\pi) \int d\epsilon f_{\ell}(\epsilon) \text{Im}G_{\ell,\ell}^{2,r}(\epsilon)$, where the retarded Green's functions $G_{\ell,\ell}^r(\epsilon)$ and $G_{\ell,\ell}^{2,r}(\epsilon)$ are given in Eqs. (A.16) and (A.17). They are solved self-consistently. We find that the resonant channels of $\mathcal{A}_{\ell,j}$ are related to the off-diagonal one-particle Green's function, which is given by

$$\begin{aligned} G_{\ell,j}^r(\epsilon)/t_{12} &= \frac{p_1}{\mu_{\ell}\mu_j - t_{12}^2} + \frac{p_2}{(\mu_{\ell} - U_{\ell,j})(\mu_j - U_j) - t_{12}^2} \\ &+ \frac{p_3}{(\mu_{\ell} - U_{\ell,j})(\mu_j - U_{j,\ell}) - t_{12}^2} \\ &+ \frac{p_4}{(\mu_{\ell} - 2U_{\ell,j})(\mu_j - U_j - U_{j,\ell}) - t_{12}^2} \\ &+ \frac{p_5}{(\mu_{\ell} - U_{\ell})(\mu_j - U_{j,\ell}) - t_{12}^2} \\ &+ \frac{p_6}{(\mu_{\ell} - U_{\ell} - U_{\ell,j})(\mu_j - U_j - U_{j,\ell}) - t_{12}^2} \\ &+ \frac{p_7}{(\mu_{\ell} - U_{\ell} - U_{\ell,j})(\mu_j - 2U_{j,\ell}) - t_{12}^2} \\ &+ \frac{p_8}{(\mu_{\ell} - U_{\ell} - 2U_{\ell,j})(\mu_j - U_j - 2U_{j,\ell}) - t_{12}^2}. \end{aligned} \quad (6)$$

To study thermoelectric properties in the linear response regime, we rewrite Eq. (2) as

$$J = \mathcal{L}_{11}\Delta V + \mathcal{L}_{12}\Delta T, \quad (7)$$

where $\Delta T = T_L - T_R > 0$ is the temperature difference between two electrodes. Coefficients in Eq. (7) are given by

$$\begin{aligned} \mathcal{L}_{11} &= \frac{2e^2}{h} \int d\epsilon \mathcal{T}(\epsilon) \left(\frac{\partial f(\epsilon)}{\partial E_F} \right)_T, \\ \mathcal{L}_{12} &= \frac{2e}{h} \int d\epsilon \mathcal{T}(\epsilon) \left(\frac{\partial f(\epsilon)}{\partial T} \right)_{E_F}. \end{aligned} \quad (8)$$

Here $\mathcal{T}(\epsilon)$ and $f(\epsilon) = 1/[e^{(\epsilon - E_F)/k_B T} + 1]$ are evaluated at thermal equilibrium. If the system is in an open circuit, the electrochemical potential (ΔV) will be established in response to a temperature gradient; this electrochemical potential is known as the Seebeck voltage. The Seebeck coefficient is defined as $S = \Delta V/\Delta T = -\mathcal{L}_{12}/\mathcal{L}_{11}$, where \mathcal{L}_{11} denotes the electrical conductance G_e .

III. RESULTS AND DISCUSSIONS

A. Current rectification and NDC

To calculate the tunneling current of SCQD, we adopt the following physical parameters: $U_{\ell} = 30\Gamma_0$, $U_{12} = 10\Gamma_0$, and $E_1 = E_F - 10\Gamma_0$, where Γ_0 is a convenient energy unit. To simplify analysis, we ignore the magnitude fluctuation of on-site Coulomb interactions and take

$U_{\ell} = U_0 = 30\Gamma_0$. The energy level of dot 2 (E_2) is tunable. $\eta_{1(2)}e\Delta V_a$ is employed to describe the energy shift arising from the applied voltage ΔV_a across the junction.² That means that E_{ℓ} is replaced by $E_{\ell} + \eta_{\ell}e\Delta V_a$, **assuming the right lead is grounded**. Although the factor η_{ℓ} depends on the QD shape, material dielectric constant, and location, we assume that η_{ℓ} is determined by the QD location, **that is**, $\eta_{\ell} = L_{\ell}/L$, where L_{ℓ} is distance between the grounded electrode and the ℓ th QD, and L is the separation between the left electrode and the right electrode. **We assume $\eta_1 = 0.6$ and $\eta_2 = 0.4$. This energy level shift arising from the applied bias as observed in the experiment of Ref. 2 has been ignored by most theoretical studies of SCQD.**⁸⁻¹⁷

When the value of orbital offset $\Delta E = E_1 - E_2$ is taken to be $U_2 - U_{12}$ at $e\Delta V_a = 0$, this would satisfy a resonant tunneling condition through the spin-singlet channel [the second channel of Eq. (3)]. It is very difficult to set up SCQD in the resonant condition of $E_1 + U_{12} = E_2 + U_2$ from experimental point of view,² because **fluctuation of QD size and uncertainty of its location are hard to avoid** in the self-assembled semiconductor SCQD.² To reveal the behavior of SCQD in the off-resonance condition, we show the tunneling current as a function of applied bias for different strengths of interdot Coulomb interactions in Fig. 1. The dashed lines with triangle marks are calculated by including only the resonant function for the resonant channel, i.e.

$$\begin{aligned} \mathcal{A}_{12} &= t_{12}^2 \frac{p_2}{|(\mu_1 - U_{12})(\mu_2 - U_2) - t_{12}^2|^2}, \\ \mathcal{A}_{21} &= t_{12}^2 \frac{p_5}{|(\mu_2 - U_2)(\mu_1 - U_{12}) - t_{12}^2|^2}. \end{aligned} \quad (9)$$

This resonant function has two poles

$$E_{\pm} = \frac{\epsilon_1 + \epsilon_2 + i\Gamma \pm \sqrt{(\epsilon_2 - \epsilon_1 + i\Delta\Gamma)^2 + 4t_{12}^2}}{2}, \quad (10)$$

where $\epsilon_1 = E_1 + U_{12} + \eta_1 e\Delta V_a$, $\epsilon_2 = E_2 + U_2 + \eta_2 e\Delta V_a$, $\Gamma = (\Gamma_L + \Gamma_R)/2$, and $\Delta\Gamma = (\Gamma_L - \Gamma_R)/2$. Under the resonant condition $E_2 + U_2 = E_1 + U_{12}$, we have $E_{\pm} = E_F + i\Gamma \pm t_{12}$ at zero bias ($\Delta V_a = 0$). Bonding and antibonding states are formed due to the coupling of QDs (t_{12}). We see that the dashed line matches very well with the black solid line (obtained with the full calculation) in small bias regime. This indicates that the tunneling current is mainly contributed by the spin-singlet resonant channel while the spin-triplet channel is fully suppressed. However, we find appreciable leakage current (J_l) at high bias due to contribution through other channels. For $U_{12} \neq 10\Gamma_0$, the tunneling current in the reverse bias is seriously suppressed. The maximum current in the forward bias is shifted to higher bias. Such behaviors are attributed to **the fact** that $\epsilon = E_1 + U_{12}$ is below $\epsilon = E_2 + U_2$ in the absence of applied bias and **for** negligible t_{12} . The agreement between the dashed line with triangle marks and the solid line becomes worse when $U_{12} = 6\Gamma_0$. The results of Fig. 1 imply that deviating

from the resonant condition of $E_1 + U_{12} = E_2 + U_2$ will suppress the Pauli spin blockade for electron transport in SCQD, which plays a significant role in the application of spin filter.^{11–14} When **the resonant condition is met**, the maximum current at a voltage marked by $V_{R,max}$ (at reverse bias) is larger than that marked by $V_{F,max}$ (at forward bias), their ratio is $J_{R,max}/J_{F,max} \approx 2$. This is in quantitative agreement with experimental results reported in Ref. 2. Note that the ratio between such two maximum currents was reported and analyzed in Ref. 11.

Figure 2 shows the tunneling current as a function of applied bias for different temperatures with (a) $E_1 = E_2 = E_0 = E_F - 10\Gamma_0$ (symmetric case) and (b) $E_1 - E_2 = U_2 - U_{12}$ (asymmetric case). From Fig. 2, we see that the current rectification of SCQD arises from the symmetry breaking of the carrier transport process due to spin blockade. This mechanism was already illustrated using the master equation method in Ref. 11. We found that the ratio of reverse to forward bias maximum current ($J_{R,max}/J_{F,max}$) depends on temperature. $J_{R,max}/J_{F,max}$ is 2.1, 1.89, and 1.74 for $k_B T = 1\Gamma$, $k_B T = 1.5\Gamma_0$ and $k_B T = 2\Gamma_0$, respectively, and the maximum forward (reverse) current occurs at $e\Delta V_a = 2.8\Gamma_0$, $3.4\Gamma_0$, and $3.6\Gamma_0$ ($e\Delta V_a = -4.4\Gamma_0$, $-5\Gamma_0$, and $-5.4\Gamma_0$). So far, such temperature-dependent current rectification effects have not been reported experimentally and theoretically.

In Fig. 2, we also notice a negative differential conductance (NDC) behavior. NDC occurs when the applied bias is larger than $V_{F,max}$ ($V_{R,max}$) in the forward (reverse) bias regime. This NDC is attributed to the off-resonance behavior of QD energy levels, which can be tuned by the applied bias ($e\Delta V_a$). Therefore, it is expected that NDC can still be observed in the absence of interdot Coulomb interactions. Such a NDC behavior is similar to the case of serially coupled quantum well, but different from the case with interdot Coulomb interactions.^{14,28} The coherent tunneling current is almost **insensitive** to temperature in high bias regime, which leads to a nonthermal broadening effect of the tunneling current.^{5,6} In general, inelastic assisting tunneling due to phonons should also be considered for a full analysis of the temperature or bias dependence.¹³ It is worth noting that the NDC behavior of SCQD was also theoretically studied by several workers.^{29–33} The NDC behavior of SCQD shown in Fig. 2 can be explained by the alignment of the dot energy levels³³: the current is high when the energy levels of different dots are aligned, but is low when the alignment is off. In Ref. 33, the authors also clearly illustrated how their NDC mechanism is different from those proposed in Refs. [29–32].

B. Charge ratchet effect

So far, we have studied the charge transport properties of a single SCQD. However, it is necessary to consider the multiple SCQDs to achieve high spin current¹⁴ or to cre-

ate spin entanglement current³⁴ in the spin filter application. Therefore, the proximity effect between SCQDs arising from the inter-dot hopping and electron Coulomb interactions should be included. To derive the resonant function ($\mathcal{A}_{\ell,j}$) of multiple **SCQDs** in general based on the equation-of-motion method would be quite complicated. However, in the weak interdot hopping limit, we can apply our previous work²⁸ to construct the resonant function, $\mathcal{A}_{\ell,j}$ of multiple SCQDs by considering interdot Coulomb interactions **for** all dots,¹⁹ while keeping the interdot hopping only between levels ℓ and j . When a third dot j' (or a charge trap impurity state) is included, the resonant function for the 3-dot system can be written as

$$\mathcal{A}_{\ell,j}(\epsilon) = t_{\ell,j}^2 (\hat{a}_{j'} + \hat{b}_{j'} + \hat{c}_{j'}) \sum_m p_m / |\Pi_m|^2; \ell \neq j \neq j'. \quad (11)$$

Here the operators $\hat{a}_{j'}$, $\hat{b}_{j'}$ and $\hat{c}_{j'}$ are defined differently as in our previous work,²⁸ since we are considering the effects of adding a level rather than removing a level as in Ref. 28. Operator $\hat{a}_{j'}$ acting on the terms that follow would introduce a multiplication factor $a_{j'} = 1 - \langle n_{j',\sigma} \rangle - \langle n_{j',\bar{\sigma}} \rangle + c_{j'}$ and leave the denominator unchanged (corresponding to adding an empty dot j'). Operator $\hat{b}_{j'}$ would introduce a multiplication factor $b_{j'} = b_{j'\sigma} + b_{j'\bar{\sigma}}$ and replace μ_ℓ and μ_j in the denominator by $\mu_\ell + U_{\ell,j'}$ and $\mu_j + U_{j,j'}$, respectively (corresponding to adding a singly occupied dot j'). Operator $\hat{c}_{j'}$ would introduce a multiplication factor $c_{j'}$ and replace μ_ℓ and μ_j in the denominator by $\mu_\ell + 2U_{\ell,j'}$ and $\mu_j + 2U_{j,j'}$, respectively (corresponding to adding a doubly occupied dot j'). Similarly, the effect of adding another dot j'' can be obtained by introducing another operator ($\hat{a}_{j''} + \hat{b}_{j''} + \hat{c}_{j''}$) to obtain the expression of $\mathcal{A}_{\ell,j}(\epsilon)$ for the 4-dot system. The procedure can be repeated for adding arbitrary number of dots.

Figure 3 shows the tunneling current of two parallel SCQDs as a function of applied bias at $k_B T = 1\Gamma_0$ for energy levels with $E_\ell = E_0 = E_F - 10\Gamma_0$; $\ell = 1, 2, 3, 4$ (symmetric case). $\eta_1 = \eta_3$ and $\eta_2 = \eta_4$ are 0.6 and 0.4, respectively. The first SCQD consists of dots 1 and 2. The second SCQD consists of dots 3 and 4 with dot 3 adjacent to dot 2, while dot 4 adjacent to dot 1. Therefore, the hopping terms t_{13} and t_{24} are ignored. The inter-SCQD electron Coulomb interactions are turned off in Fig. 3. Because space symmetry is maintained, the current spectrum is symmetrical. Comparing with Fig. 2(a), we found that there is an extra peak in the forward (**reverse**) bias labeled by $J_{F2,max}$ ($J_{R2,max}$) resulting from the electron tunneling between SCQDs (labeled J_{14} and J_{23}). The various contributions to the total tunneling current of Fig. 3(a) are shown in Figs. 3(b) and 3(c). Fig. 3(b) shows that there are two resonant channels with $\epsilon_1 + U_{12} = \epsilon_4 + U_{34}$ and $\epsilon_1 = \epsilon_4 + 2U_{34}$, where $\epsilon_\ell = E_\ell + \eta_\ell e\Delta V_a$. The second peak at the bias ($e\Delta V_a = 50\Gamma_0$) results from electron in state E_1 tunneling to state $E_4 + 2U_{34}$. From **the** electron occupation numbers ($N_1 = N_3$ and $N_2 = N_4$) shown in Fig. 3(d),

we see that the probabilities of two electrons in E_3 and empty E_4 are high under forward bias; therefore, the resonant channel of $\varepsilon_4 + 2U_{34}$ is yielded. Because the SCQD is symmetric, the resonant channels under reverse bias are the same as those under forward bias.

Figure 4 shows the tunneling current of two parallel SCQDs as a function of applied bias at $k_B T = 1\Gamma_0$ for the asymmetric case ($E_1 - E_2 = U_2 - U_{12}$). Unlike the symmetrical case of Fig. 3, the SCQD is in the spin singlet state. The maximum current labeled by $J_{F1,max}$ and $J_{R1,max}$ are not only from **intra-SCQD**, but also from inter-SCQD channels. These two separate contributions are illustrated in Figs. 4(b) and 4(c). The resonant channels at the conditions $\varepsilon_1 + U_1 = \varepsilon_4 + U_4 + 2U_{34}$ and $\varepsilon_4 + U_4 = \varepsilon_1 + 2U_{12}$ correspond to the current maxima labeled by $J_{F2,max}$ and $J_{R2,max}$, respectively. We note that the ratio of $J_{R2,max}/J_{F2,max}$ (due to inter-SCQD tunneling) is much larger than the ratio $J_{R1,max}/J_{F1,max}$ (due to intra-SCQD tunneling). This is attributed to the direction-dependent probability factors, which are determined by the occupation numbers shown in Fig. 4(d). Highly asymmetric behavior of these occupation numbers is noticed. $N_1 = N_3$ is almost empty under high reversed bias, which leads to a large probability weight for electrons entering level E_4 (E_2) and tunneling through level E_1 (E_3). So far, we have not taken into account the inter-SCQD Coulomb interactions in Figs. (3) and (4). In a realistic **system with** two parallel SCQDs, the **inter-SCQD** electron Coulomb interactions will significantly influence the current spectrum. Figure 5 shows the effects due to the presence of inter-SCQD Coulomb interactions. Here, we consider $U_{13} = U_{24} = 5\Gamma_0$ and $U_{14} = U_{23} = 3\Gamma_0$. The current rectification in the low bias regime ($e\Delta V_a \leq 12\Gamma_0$) which **exists** for isolated SCQD is now completely washed out, because the resonant condition of $E_1 + U_{12} = E_2 + U_2$ no longer holds. In addition, the current spectrum is seriously suppressed under the **reverse** bias. Now, the maximum currents $J_{F1,max}$ and $J_{F2,max}$ result from the channels $\varepsilon_1 + U_{12} + U_{14} = \varepsilon_4 + U_4 + U_{24}$ and $\varepsilon_1 + U_1 = \varepsilon_4 + U_4 + U_{34}$. The occupation numbers are shown in Fig. 5(d), which are useful for the analysis of charge state in each QD. The results of Fig. 5 imply that to control the spin charge configuration of multiple SCQDs, the proximity effect should be carefully taken into account.

Recently, Si SCQDs attract serious attention for quantum bit applications due to their small nuclear-electron spin interaction.^{21,22} Although Si SCQDs may have a longer spin relaxation time, two issues need to be addressed: (i) The multi-valleyed nature of the Si conduction band leads to several closely spaced energy levels in a Si QD. For a spherical Si QD, the six degenerate valleys can be mixed by the confining potential to form A_1 -symmetry (1 fold), T_2 -symmetry (3-fold) and E -symmetry (2-fold) states. The degeneracies may be further lifted by any deviation from the spherical shape. (ii) The presence of defect charge trap states in the oxide surrounding of Si QDs. In order to understand how

these two issues influence the current rectification, one needs to calculate the **resonant function** of SCQD with closely spaced multiple energy levels. Here, we consider a SCQD with two energy levels per dot (E_1 and E_3 in dot 1 and E_2 and E_4 in dot 2). Figure 6 shows the tunneling current at $k_B T = 1\Gamma_0$ as a function of applied bias for various values of E_3 . When E_3 and E_4 are above and far away from E_F , the current rectification of SCQD is not affected [as shown in 6(a)], because these levels are unoccupied for all applied voltages considered. When E_3 is within a couple of Γ_0 from E_F , there exist several peaks in the high bias regime as labeled by $J_{F2,max}$, $J_{R2,max}$, and $J_{F3,max}$. Note that E_3 is still above E_F , and the ratio $J_{R1,max}/J_{F1,max}$ is changed only slightly. Meanwhile, the voltages corresponding to the maximum current, $J_{F1,max}$ and $J_{R1,max}$ are also nearly unchanged and stay close to $2\Gamma_0$ and $-2.5\Gamma_0$. When $E_3 = E_F - \Gamma_0$, a shoulder labeled $J_{R2,max}$ appears near the first peak $J_{R1,max}$ under reverse bias. The voltage corresponding to maximum current, $J_{R1,max}$ is shifted to high voltage ($-3\Gamma_0$) as a result of the charge ratchet effect due to levels 3 and 4 (the asymmetrical behavior of N_3 and N_4 not shown here). The resonant channels of the current spectrum shown in Fig. 6(c) can be analyzed as follows: The resonant peaks labeled $J_{F1,max}$ and $J_{R1,max}$ arise from electrons tunneling between level E_1 and E_2 . Electrons tunneling between levels E_3 and E_4 give rise to the peak labeled by $J_{F3,max}$. Peaks labeled by $J_{F2,max}$ and $J_{R2,max}$ arise from electron tunneling between levels E_3 and E_2 . The analysis of Fig. 6 infers that the Pauli spin blockade condition of the Si SCQD^{21,22} and the spin entanglement current of triple quantum dots³⁴ may not be readily implemented due to the fluctuations of electron Coulomb interactions and energy levels in each QD.

C. Thermoelectric properties

In this section, we examine the effect of spin blockade on the thermoelectric properties of SCQDs. To realize the resonant condition in the Pauli spin blockade regime in a SCQD junction can be challenging due to size fluctuation of QDs and uncertain distances between the fabricated QDs. In general, gate electrodes are used to tune the energy level of each QD to help realize the resonant condition. Figure 7 shows (a) **the electrical conductance (G_e)** and (b) **Seebeck coefficient (S)** of SCQD with $E_1 = E_F - 10\Gamma_0$ and $E_2 = E_F + 20\Gamma_0 - eV_g$ as functions of gate voltage **and temperature**. The gate voltage is applied only to dot B. In Fig. 7(a), the four gate voltages V_{g1} , V_{g2} , V_{g3} , and V_{g4} tune the energy level of dot B (E_2) to E_F , $E_F - U_{12}$, $E_F - U_2$ and $E_F - U_2 - U_{12}$, respectively to match different **resonant** channels for the electron entering through $E_1 + U_{12}$. The temperature dependence of the peaks at V_{g2} and V_{g3} displays a nonthermal broadening effect on the electrical conductance. These two peaks correspond to the resonances for the spin-triplet (at $eV_g = 30\Gamma_0$) spin-singlet (at $eV_g = 50\Gamma_0$) states, re-

spectively. It is worth noting that the magnitude of G_e is much smaller than $2e^2/h$, which manifests the effect of electron Coulomb interactions. In the absence of electron Coulomb interactions we would have $G_e = 2e^2/h$, because the sum of probability weights of resonant channels would equal to one. The peak heights of these resonances decrease with increasing temperature, while the widths are not sensitive to temperature. This behavior was first reported in the tunneling current measurement of SCQD in Refs. 5 and 6. Theoretical work for the nonthermal broadening of G_e was previously investigated only for the **noninteracting system**.³⁵ A simple explanation for the nonthermal broadening effect is that the broadening of the tunneling current under the double-resonance condition is determined by the smaller-scale tunneling rates $\Gamma_{1,2}$ and interdot coupling t_{12} , therefore is not sensitive to the larger-scale temperature variation in the distribution functions $f_{L,R}$. The nonthermal broadening behavior of G_e can be useful in the application for low-temperature current filtering. Our results demonstrate that a SCQD can function as a spin filter and low-temperature current filter at the same time. **The two tiny peaks labeled by V_{g1} and V_{g4} may not be resolved in the measurement of electrical conductance G_e .** However, they can be resolved in the measurement of Seebeck coefficient S as illustrated in Fig. 7(b). In addition, the Seebeck coefficient also shows a sign change with respect to applied gate voltage near the resonances, which arises from the bipolar effect, **as** shall be explained in details below. The inhomogeneous shape of S is very different from the symmetrical sawtooth shape for a single metallic QD.²⁶

In Ref. 24, the electrical conductance G_e and Seebeck coefficient S of a single QD with two energy levels were theoretically investigated. In the case of **two identical quantum dots coupled together**, Eq. (2) can also be used to reveal the behavior of G_e and S . Figure 8 shows (a) G_e and (b) S of a SCQD with $E_1 = E_2 = E_F - 10\Gamma_0$ (symmetric case) as functions of gate voltage (applied to both dots) and temperature. In Fig. 8(a), the four gate voltages V_{g1} , V_{g2} , V_{g3} , and V_{g4} tune the energy levels of both dots ($E_1 = E_2$) to E_F , $E_F - U_{12}$, $E_F - U_2$ and $E_F - U_2 - U_{12}$, while the SCQD is filled with one, two (quantum dot “helium” case), three, and four electrons, respectively. These peaks become broadened with increasing temperature, unlike in the asymmetric case of Fig. 7. The results of Fig. 8(a) are similar to the typical thermal broadening behavior of a single dot with multiple energy levels.²⁴ It is noticed that **S** goes through zero when G_e reaches a maximum or minimum (which occurs midway between two G_e peaks). The positions of zero **S** are not affected by the temperature variation. Such a behavior is different from that of Fig. 7(b). In addition, the shape of S is also different from the sawtooth shape of metallic QDs with homogenous electron Coulomb interactions. We note that **G_e and S** in the symmetric case (Fig. 8) are larger than that of asymmetric case (Fig. 7). The above analysis should be useful for the optimization of the figure of merit for thermoelectric property.^{23,24}

Figure 9 shows the electrical conductance G_e and Seebeck coefficient S as a function of temperature for two arrangements of SCQDs: (a) asymmetric case with $E_1 - E_2 = U_2 - U_{12}$ (solid lines) and (b) symmetric case with $E_1 = E_2 = E_F - 10\Gamma_0$ (dashed lines). Based on Eq. (3), these two cases denote the spin singlet [inset of Fig. 9(a)] and triplet states [inset of Fig. 9(b)], respectively. It is not easy to distinguish the singlet and triplet states from the electrical conductance as **a function** of temperature, because the electrical conductance difference in singlet and triplet states is small. However, the Seebeck coefficient provides **an** easy means to distinguish the spin singlet and triplet states, since the sign of Seebeck coefficient changes for the spin triplet state as temperature increases, but for the spin singlet state, the Seebeck coefficient is always negative, because the electrons from the left electrode (hot side) diffuse into the right electrode (cold side) through the resonant channels above the Fermi energy, which leads to the built-up of negative ΔV in order to reach the $J = 0$ condition for open circuit. Note that the resonant channel of $E_1 + U_{12} = E_2 + U_2$ has no contribution to the Seebeck coefficient ($\mathcal{L}_{12} = 0$). **For the spin triplet state, zero Seebeck coefficient occurs at T_0 , i.e. $S(T_0) = 0$,** which indicates that the current arising from temperature gradient can be self-balanced without electrochemical potential ($\Delta V = 0$). On the other hand, the Seebeck coefficient is positive when **the holes** from the left electrode (hot side) diffuse into the right electrode (cold side) via the resonant channels below E_F . Here, we have defined the unoccupied states below E_F as holes. Consequently, the sign change in S is attributed to the competition between tunneling currents due to electrons and holes (**so-called bipolar effect**). This implies that we can control the current direction by **manipulating** the equilibrium temperature. In addition, we can distinguish the spin singlet and triplet states by measuring the temperature dependence of the Seebeck coefficient.

IV. SUMMARY

We have used a two-level Anderson model to describe **a** SCQD connected to metallic electrodes and calculated the tunneling current within the framework of nonequilibrium Green’s function technique. In the Coulomb blockade regime, we have derived a closed-form expression for tunneling current. In the nonlinear response regime, the electron spin singlet and triplet states can be distinguished by the current rectification behavior arising from the space symmetry breaking, whereas such a current rectification effect in the spin blockade process is suppressed with increasing temperature. We have also studied the proximity effect between two parallel SCQDs and analyzed how the charge trapping states influence the current rectification of SCQD. In the linear response regime, the electrical conductance G_e and Seebeck coefficient S are analyzed. It is not easy to distinguish

G_e due to transport through the spin singlet or triplet states from its temperature behavior. **However**, the temperature dependence of Seebeck coefficient can clearly reveal the spin configuration by examining the sign of S . For example, we observe a sign change in S for electron transport through the spin triplet states, while S is always negative for transport through the spin singlet state. Thus, we conclude that the measurement of Seebeck coefficient provides a much better means for resolving the resonant channels than measuring the electrical conductance. In addition, we see a nonthermal broadening effect of tunneling current for the spin blockade process. This indicates that SCQD can simultaneously act as the spin filter and low-temperature current filter.

Acknowledgments- This work was supported in part by the National Science Council of the Republic of China under Contracts 99-2112-M-008-018-MY2, 99-2120-M-008-004-MY3, and 98-2112-M-001-022-MY3.

Appendix A.

The expression of the tunneling current through serially coupled quantum dots (SCQD) is derived based on the seminal work by Meir and Wingreen⁷. J_L and J_R denote, respectively, the tunneling current of electrons leaving the left and right electrodes, which are expressed by

$$J_L = \frac{-e}{h} \int d\epsilon \Gamma_1(\epsilon) [2f_L(\epsilon) \text{Im} G_{1,1}^r(\epsilon) - iG_{1,1}^<(\epsilon)], \quad (\text{A.1})$$

and

$$J_R = \frac{-e}{h} \int d\epsilon \Gamma_2(\epsilon) [2f_R(\epsilon) \text{Im} G_{2,2}^r(\epsilon) - iG_{2,2}^<(\epsilon)]. \quad (\text{A.2})$$

According to expressions of Eqs. (A.1) and (A.2), tunneling current is determined by the on-site retarded and lesser Green's functions (GFs). Note that we consider the SCQD system to be spin degenerate, thus have suppressed the spin index for convenience. Here $G_{\ell,j}^r(t) \equiv -i\theta(t)\langle\{d_{\ell,\sigma}(t), d_{j,\sigma}^\dagger\}\rangle$ and its Fourier transform $G_{\ell,j}^r(\epsilon) = \langle d_{\ell,\sigma} | d_{j,\sigma}^\dagger \rangle$ denote the one-particle GF.

It is nontrivial to obtain an exact solution of $G_{\ell,j}^r(\epsilon)$ for the system Hamiltonian when the coupling with leads is present.¹⁴ We solve the on-site retarded and lesser GFs in the Coulomb blockade regime. One-particle GF $G_{\ell,j}^r(\epsilon)$ can be obtained by solving a closed set of equations of motion. For coupled QDs, it is convenient to define vector GFs as

$$\mathcal{G}^{(1)} = \begin{pmatrix} \langle d_{1\sigma} | d_{1\sigma}^\dagger \rangle \\ \langle d_{2\sigma} | d_{1\sigma}^\dagger \rangle \end{pmatrix}, \quad \mathcal{G}_i^{(2)} = \begin{pmatrix} \langle n_{i\bar{\sigma}} d_{1\sigma} | d_{1\sigma}^\dagger \rangle \\ \langle n_{i\bar{\sigma}} d_{2\sigma} | d_{1\sigma}^\dagger \rangle \end{pmatrix},$$

$$\mathcal{G}_3^{(2)} = \begin{pmatrix} \langle n_{2\sigma} d_{1\sigma} | d_{1\sigma}^\dagger \rangle \\ \langle n_{1\sigma} d_{2\sigma} | d_{1\sigma}^\dagger \rangle \end{pmatrix}, \quad \mathcal{G}_i^{(3)} = \begin{pmatrix} \langle n_{2\sigma} n_{i\bar{\sigma}} d_{1\sigma} | d_{1\sigma}^\dagger \rangle \\ \langle n_{1\sigma} n_{i\bar{\sigma}} d_{2\sigma} | d_{1\sigma}^\dagger \rangle \end{pmatrix};$$

$$i=1,2,12, \text{ or } 21, \quad \mathcal{G}_3^{(3)} = \begin{pmatrix} \langle n_{2\bar{\sigma}} n_{1\bar{\sigma}} d_{1\sigma} | d_{1\sigma}^\dagger \rangle \\ \langle n_{2\bar{\sigma}} n_{1\bar{\sigma}} d_{2\sigma} | d_{1\sigma}^\dagger \rangle \end{pmatrix}, \text{ and}$$

$$\mathcal{G}^{(4)} = \begin{pmatrix} \langle n_{2\bar{\sigma}} n_{2\sigma} n_{1\bar{\sigma}} d_{1\sigma} | d_{1\sigma}^\dagger \rangle \\ \langle n_{2\bar{\sigma}} n_{1\bar{\sigma}} n_{1\sigma} d_{2\sigma} | d_{1\sigma}^\dagger \rangle \end{pmatrix}, \text{ where the superscripts denote the number of particles involved, and we have de-}$$

fined $n_{\ell j \bar{\sigma}} = d_{\ell \bar{\sigma}}^\dagger d_{j \bar{\sigma}}$; $\ell, j = 1, 2$. $\bar{\sigma}$ denotes the opposite of spin σ .

From Eq. (1) we obtain the equations of motion that relate $\mathcal{G}^{(1)}$ to $\mathcal{G}^{(2)}$'s, then to $\mathcal{G}^{(3)}$'s, and finally to $\mathcal{G}^{(4)}$, which self-terminates. The one-particle GFs satisfy

$$\mathcal{H}_0 \mathcal{G}^{(1)} = \begin{pmatrix} 1 \\ 0 \end{pmatrix} + \mathcal{U} \mathcal{G}_1^{(2)} + \tilde{\mathcal{U}} \mathcal{G}_2^{(2)} + U_{12} \mathcal{G}_3^{(2)}, \quad (\text{A.3})$$

where we have defined $\mathcal{H}_0 = \begin{pmatrix} \mu_1 & -t_{12} \\ -t_{12} & \mu_2 \end{pmatrix}$, $\mu_\ell = \epsilon - E_{\ell,\sigma} + i\Gamma_\ell/2$; $\ell = 1, 2$ ($\Gamma_\ell = 2\pi \sum_{\mathbf{k}} |V_{\mathbf{k},\ell}|^2 \delta(\epsilon - \epsilon_{\mathbf{k}})$) arising from the QD coupled to electrode), $\mathcal{U} = \begin{pmatrix} U_1 & 0 \\ 0 & U_{12} \end{pmatrix}$, and $\tilde{\mathcal{U}} = \begin{pmatrix} U_{12} & 0 \\ 0 & U_2 \end{pmatrix}$. The two-particle GFs satisfy

$$(\mathcal{H}_0 - \mathcal{U}) \mathcal{G}_1^{(2)} = \begin{pmatrix} N_{1\bar{\sigma}} \\ 0 \end{pmatrix} + t_{12} (\mathcal{G}_{12}^{(2)} - \mathcal{G}_{21}^{(2)}) + \tilde{\mathcal{U}} \mathcal{G}_3^{(3)} + U_{12} \mathcal{G}_1^{(3)}, \quad (\text{A.4})$$

$$(\mathcal{H}_0 - \tilde{\mathcal{U}}) \mathcal{G}_2^{(2)} = \begin{pmatrix} N_{2\bar{\sigma}} \\ 0 \end{pmatrix} - t_{12} (\mathcal{G}_{12}^{(2)} - \mathcal{G}_{21}^{(2)}) + \mathcal{U} \mathcal{G}_3^{(3)} + U_{12} \mathcal{G}_2^{(3)}, \quad (\text{A.5})$$

$$(\mathcal{H}_0 - U_{12}) \mathcal{G}_3^{(2)} = \begin{pmatrix} N_{2\sigma} \\ -\langle n_{12\sigma} \rangle \end{pmatrix} + \mathcal{U} \mathcal{G}_1^{(3)} + \tilde{\mathcal{U}} \mathcal{G}_2^{(3)}, \quad (\text{A.6})$$

$$(\mathcal{H}_0 - \tilde{\mathcal{U}} - \Delta\epsilon) \mathcal{G}_{12}^{(2)} = \begin{pmatrix} \langle n_{12\bar{\sigma}} \rangle \\ 0 \end{pmatrix} + t_{12} (\mathcal{G}_1^{(2)} - \mathcal{G}_2^{(2)}) + \mathcal{U}' \mathcal{G}_{12}^{(3)}, \quad (\text{A.7})$$

$$(\mathcal{H}_0 - \mathcal{U} + \Delta\epsilon) \mathcal{G}_{21}^{(2)} = \begin{pmatrix} \langle n_{21\bar{\sigma}} \rangle \\ 0 \end{pmatrix} - t_{12} (\mathcal{G}_1^{(2)} - \mathcal{G}_2^{(2)}) - \mathcal{U}' \mathcal{G}_{21}^{(3)}, \quad (\text{A.8})$$

where $\Delta\epsilon = E_2 - E_1$ and $\mathcal{U}' = \begin{pmatrix} U_2 & 0 \\ 0 & -U_1 \end{pmatrix}$.

The three-particle GFs satisfy

$$(\mathcal{H}_0 - \mathcal{U} - U_{12}) \mathcal{G}_1^{(3)} = \begin{pmatrix} c_{2\sigma,1\bar{\sigma}} \\ -c_{12\sigma,1\bar{\sigma}} \end{pmatrix} + \tilde{\mathcal{U}} \mathcal{G}^{(4)}, \quad (\text{A.9})$$

$$(\mathcal{H}_0 - \tilde{\mathcal{U}} - U_{12}) \mathcal{G}_2^{(3)} = \begin{pmatrix} c_2 \\ -c_{12\sigma,2\bar{\sigma}} \end{pmatrix} + \mathcal{U} \mathcal{G}^{(4)}, \quad (\text{A.10})$$

$$(\mathcal{H}_0 - \mathcal{U} - \tilde{\mathcal{U}}) \mathcal{G}_3^{(3)} = \begin{pmatrix} c_{2\bar{\sigma},1\bar{\sigma}} \\ 0 \end{pmatrix} + U_{12} \mathcal{G}^{(4)}, \quad (\text{A.11})$$

$$\begin{pmatrix} \mu_1 - \Delta\epsilon - U_2 - U_{12} & -t_{12} \\ -t_{12} & \mu_2 - \Delta\epsilon - U_2 + U_1 - 2U_{12} \end{pmatrix} \mathcal{G}_{12}^{(3)} \\ = \begin{pmatrix} c_{2\sigma,12\bar{\sigma}} \\ -c_{12} \end{pmatrix} + t_{12} (\mathcal{G}_1^{(3)} - \mathcal{G}_2^{(3)}), \quad (\text{A.12})$$

$$\begin{pmatrix} \mu_1 + \Delta\epsilon - U_1 + U_2 - 2U_{12} & -t_{12} \\ -t_{12} & \mu_2 + \Delta\epsilon - U_1 - U_{12} \end{pmatrix} \mathcal{G}_{21}^{(3)} \\ = \begin{pmatrix} c_{2\sigma,21\bar{\sigma}} \\ -c_{12\sigma,21\bar{\sigma}} \end{pmatrix} - t_{12} (\mathcal{G}_1^{(3)} - \mathcal{G}_2^{(3)}), \quad (\text{A.13})$$

where we have defined the c-numbers $c_i = \langle n_{i,\sigma} n_{i,\bar{\sigma}} \rangle$, and $c_{i\sigma,i'\sigma'} = \langle n_{i\sigma} n_{i'\sigma'} \rangle$; $i, i' = 1, 2, 12, 21$. Finally, the four-particle GFs satisfy

$$(\mathcal{H}_0 - \mathcal{U} - \tilde{\mathcal{U}} - U_{12}) \mathcal{G}^{(4)} = \begin{pmatrix} \langle n_{2\sigma} n_{2\bar{\sigma}} n_{1\bar{\sigma}} \rangle \\ -\langle n_{12\sigma} n_{2\bar{\sigma}} n_{1\bar{\sigma}} \rangle \end{pmatrix}. \quad (\text{A.14})$$

From Eqs. (A.4) and (A.5), we see that the terms $\mathcal{G}_{12}^{(2)}$ and $\mathcal{G}_{21}^{(2)}$ only give a small correction of order t_{12}^2/U to $\mathcal{G}_1^{(2)}$ and $\mathcal{G}_2^{(2)}$, while those off-diagonal expectation values such as $\langle n_{12\sigma} \rangle$ that are of the first order in t_{12} in Eq. (A.6) give a correction of t_{12}/U ; thus, these terms can be ignored in the limit of small t_{12}/U . If we further make the approximation $\langle n_{2\sigma} n_{2\bar{\sigma}} n_{1\bar{\sigma}} \rangle = c_2 N_{1\bar{\sigma}}$ (valid again in weak **interdot** coupling case), then the one-particle GFs can be written in simple closed forms.

From Eqs.(A.3-14), we found that the one-particle retarded **GF** can be simply decomposed into a sum of contributions from eight spin-charge configurations of the SCQD system in the condition of $t_{12}/U_\ell \ll 1$ (after ignoring those small contributions proportional to t_{12}/U). It reads

$$\begin{aligned} \mathcal{G}^{(1)} = & \mathcal{H}_0^{-1} \mathcal{P}_1 + (\mathcal{H}_0 - \tilde{U})^{-1} \mathcal{P}_2 + (\mathcal{H}_0 - U_{12})^{-1} \mathcal{P}_3 \\ & + (\mathcal{H}_0 - \tilde{U} - U_{12})^{-1} \mathcal{P}_4 + (\mathcal{H}_0 - U)^{-1} \mathcal{P}_5 \\ & + (\mathcal{H}_0 - U - \tilde{U})^{-1} \mathcal{P}_6 + (\mathcal{H}_0 - U - U_{12})^{-1} \mathcal{P}_7 \\ & + (\mathcal{H}_0 - \tilde{U} - U - U_{12})^{-1} \mathcal{P}_8, \end{aligned} \quad (\text{A.15})$$

where $\mathcal{P}_m = \begin{pmatrix} p_m \\ 0 \end{pmatrix}$; p_m 's are probability weights defined in Eq. (3). The intradot one-particle and two-particle retarded **GFs** are given by

$$\begin{aligned} G_{\ell,\ell}^r(\epsilon) = & \frac{p_1}{\mu_\ell - t_{12}^2/\mu_j} + \frac{p_2}{(\mu_\ell - U_{\ell,j}) - t_{12}^2/(\mu_j - U_j)} \\ & + \frac{p_3}{(\mu_\ell - U_{\ell,j}) - t_{12}^2/(\mu_j - U_{j,\ell})} \\ & + \frac{p_4}{(\mu_\ell - 2U_{\ell,j}) - t_{12}^2/(\mu_j - U_j - U_{j,\ell})} \\ & + \frac{p_5}{(\mu_\ell - U_\ell) - t_{12}^2/(\mu_j - U_{j,\ell})} \\ & + \frac{p_6}{(\mu_\ell - U_\ell - U_{\ell,j}) - t_{12}^2/(\mu_j - U_j - U_{j,\ell})} \\ & + \frac{p_7}{(\mu_\ell - U_\ell - U_{\ell,j}) - t_{12}^2/(\mu_j - 2U_{j,\ell})} \\ & + \frac{p_8}{(\mu_\ell - U_\ell - 2U_{\ell,j}) - t_{12}^2/(\mu_j - U_j - 2U_{j,\ell})}, \end{aligned} \quad (\text{A.16})$$

and

$$\begin{aligned} G_{\ell,\ell}^{2,r}(\epsilon) = & \frac{p_5}{(\mu_\ell - U_\ell) - t_{12}^2/(\mu_j - U_{j,\ell})} \\ & + \frac{p_6}{(\mu_\ell - U_\ell - U_{\ell,j}) - t_{12}^2/(\mu_j - U_j - U_{j,\ell})} \\ & + \frac{p_7}{(\mu_\ell - U_\ell - U_{\ell,j}) - t_{12}^2/(\mu_j - 2U_{j,\ell})} \\ & + \frac{p_8}{(\mu_\ell - U_\ell - 2U_{\ell,j}) - t_{12}^2/(\mu_j - U_j - 2U_{j,\ell})}. \end{aligned} \quad (\text{A.17})$$

The index j denotes the j th QD, and $j \neq \ell$ in Eqs. (A.16) and (A.17).

Here we shall derive the one-particle lesser **GFs** $G_{11}^{<} <math> <math>$

where we define in 2×2 matrix form $\Sigma^{<} = \begin{pmatrix} \Sigma_1^{<} & 0 \\ 0 & \Sigma_2^{<} \end{pmatrix}$ with $\Sigma_\alpha^{<} = i\Gamma_\alpha(\epsilon)f_\alpha(\epsilon)$ for $\alpha = 1, 2$ and **one-particle advanced GF** vectors $\mathcal{G}^{a(1)}$ in Eq. (A.18). The two-particle lesser **GFs** satisfy

$$(\mathcal{H}_0 - U)\mathcal{G}_1^{<(2)} = \Sigma^{<}\mathcal{G}_1^{a(2)} + \tilde{U}\mathcal{G}_3^{<(3)} + U_{12}\mathcal{G}_1^{<(3)}, \quad (\text{A.19})$$

$$(\mathcal{H}_0 - \tilde{U})\mathcal{G}_2^{<(2)} = \Sigma^{<}\mathcal{G}_2^{a(2)} + U\mathcal{G}_3^{<(3)} + U_{12}\mathcal{G}_2^{<(3)}, \quad (\text{A.20})$$

$$(\mathcal{H}_0 - U_{12})\mathcal{G}_3^{<(2)} = \Sigma^{<}\mathcal{G}_3^{a(2)} + U\mathcal{G}_1^{<(3)} + \tilde{U}\mathcal{G}_2^{<(3)}. \quad (\text{A.21})$$

The three-particle lesser **GFs** satisfy

$$(\mathcal{H}_0 - U - U_{12})\mathcal{G}_1^{<(3)} = \Sigma^{<}\mathcal{G}_1^{a(3)} + \tilde{U}\mathcal{G}^{<(4)}, \quad (\text{A.22})$$

$$(\mathcal{H}_0 - \tilde{U} - U_{12})\mathcal{G}_2^{<(3)} = \Sigma^{<}\mathcal{G}_2^{a(3)} + U\mathcal{G}^{<(4)}, \quad (\text{A.23})$$

$$(\mathcal{H}_0 - U - \tilde{U})\mathcal{G}_3^{<(3)} = \Sigma^{<}\mathcal{G}_3^{a(3)} + U_{12}\mathcal{G}^{<(4)}. \quad (\text{A.24})$$

The four-particle lesser **GFs** satisfy

$$(\mathcal{H}_0 - U - \tilde{U} - U_{12})\mathcal{G}^{<(4)} = \Sigma^{<}\mathcal{G}^{a(4)}. \quad (\text{A.25})$$

The approximations made here conform to those at deriving the retarded **GFs** in the weak t_{12} limit. Similarly, we found that the lesser **GFs** can equally be decomposed into a sum of contributions. It reads

$$\begin{aligned} \mathcal{G}^{<(1)} = & \mathcal{H}_0^{-1}\Sigma^{<}\mathcal{H}_0^{*-1}\mathcal{P}_1 + (\mathcal{H}_0 - \tilde{U})^{-1}\Sigma^{<}(\mathcal{H}_0^* - \tilde{U})^{-1}\mathcal{P}_2 \\ & + (\mathcal{H}_0 - U_{12})^{-1}\Sigma^{<}(\mathcal{H}_0^* - U_{12})^{-1}\mathcal{P}_3 \\ & + (\mathcal{H}_0 - \tilde{U} - U_{12})^{-1}\Sigma^{<}(\mathcal{H}_0^* - \tilde{U} - U_{12})^{-1}\mathcal{P}_4 \\ & + (\mathcal{H}_0 - U)^{-1}\Sigma^{<}(\mathcal{H}_0^* - U)^{-1}\mathcal{P}_5 \\ & + (\mathcal{H}_0 - U - \tilde{U})^{-1}\Sigma^{<}(\mathcal{H}_0^* - U - \tilde{U})^{-1}\mathcal{P}_6 \\ & + (\mathcal{H}_0 - U - U_{12})^{-1}\Sigma^{<}(\mathcal{H}_0^* - U - U_{12})^{-1}\mathcal{P}_7 \\ & + (\mathcal{H}_0 - \tilde{U} - U - U_{12})^{-1}\Sigma^{<}(\mathcal{H}_0^* - \tilde{U} - U - U_{12})^{-1}\mathcal{P}_8. \end{aligned} \quad (\text{A.26})$$

Straightforward algebra leads to

$$\begin{aligned} G_{\ell,\ell}^{<}(\epsilon) = & \Sigma_1^{<} \left[\frac{p_1}{|\mu_\ell - t_{12}^2/\mu_j|^2} + \frac{p_2}{|(\mu_\ell - U_{\ell,j}) - t_{12}^2/(\mu_j - U_j)|^2} \right. \\ & + \frac{p_3}{|(\mu_\ell - U_{\ell,j}) - t_{12}^2/(\mu_j - U_{j,\ell})|^2} \\ & + \frac{p_4}{|(\mu_\ell - 2U_{\ell,j}) - t_{12}^2/(\mu_j - U_j - U_{j,\ell})|^2} \end{aligned}$$

$$\begin{aligned}
& + \frac{p_5}{|(\mu_\ell - U_\ell) - t_{12}^2/(\mu_j - U_{j,\ell})|^2} \\
& + \frac{p_6}{|(\mu_\ell - U_\ell - U_{\ell,j}) - t_{12}^2/(\mu_j - U_j - U_{j,\ell})|^2} \\
& + \frac{p_7}{|(\mu_\ell - U_\ell - U_{\ell,j}) - t_{12}^2/(\mu_j - 2U_{j,\ell})|^2} \\
& + \frac{p_8}{|(\mu_\ell - U_\ell - 2U_{\ell,j}) - t_{12}^2/(\mu_j - U_j - 2U_{j,\ell})|^2} \Big] \\
& + t_{12}^2 \Sigma_2^< \left[\frac{p_1}{|\mu_\ell \mu_j - t_{12}^2|^2} + \frac{p_2}{|(\mu_\ell - U_{\ell,j})(\mu_j - U_j) - t_{12}^2|^2} \right. \\
& + \frac{p_3}{|(\mu_\ell - U_{\ell,j})(\mu_j - U_{j,\ell}) - t_{12}^2|^2} \\
& + \frac{p_4}{|(\mu_\ell - 2U_{\ell,j})(\mu_j - U_j - U_{j,\ell}) - t_{12}^2|^2} \\
& + \frac{p_5}{|(\mu_\ell - U_\ell)(\mu_j - U_{j,\ell}) - t_{12}^2|^2} \\
& + \frac{p_6}{|(\mu_\ell - U_\ell - U_{\ell,j})(\mu_j - U_j - U_{j,\ell}) - t_{12}^2|^2} \\
& + \frac{p_7}{|(\mu_\ell - U_\ell - U_{\ell,j})(\mu_j - 2U_{j,\ell}) - t_{12}^2|^2} \\
& \left. + \frac{p_8}{|(\mu_\ell - U_\ell - 2U_{\ell,j})(\mu_j - U_j - 2U_{j,\ell}) - t_{12}^2|^2} \right]. \tag{A.27}
\end{aligned}$$

The index j in Eq. (A.27) denotes the j th QD, and $j \neq \ell$. Inserting the diagonal GFs defined by Eqs.(A.16,A.27) into Eqs. (A.1,A.2) yields

$$J_L = \frac{e}{h} \int d\epsilon [f_L(\epsilon) - f_R(\epsilon)] \Gamma_1(\epsilon) \Gamma_2(\epsilon) \mathcal{A}_{12}(\epsilon), \tag{A.28}$$

and

$$J_R = \frac{e}{h} \int d\epsilon [f_R(\epsilon) - f_L(\epsilon)] \Gamma_1(\epsilon) \Gamma_2(\epsilon) \mathcal{A}_{21}(\epsilon). \tag{A.29}$$

Furthermore, using $J = J_L = (J_L - J_R)/2$ and $J_L = -J_R$, we can symmetrize the current as

$$\mathbf{J} = \frac{2e}{h} \int d\epsilon \mathcal{T}(\epsilon) [f_L(\epsilon) - f_R(\epsilon)], \tag{A.30}$$

where we define the transmission factor

$$\mathcal{T}(\epsilon) = \Gamma_1(\epsilon) \Gamma_2(\epsilon) (\mathcal{A}_{12}(\epsilon) + \mathcal{A}_{21}(\epsilon))/2. \tag{A.31}$$

The factor 2 in Eq.(A.30) accounts for the electron spin degree of freedom. \mathcal{A}_{12} and \mathcal{A}_{21} in Eq. (A.31) are called resonant functions, which are given by

$$\mathcal{A}_{\ell,j}(\epsilon) = t_{12}^2 \sum_{m=1}^8 p_m / |\Pi_m|^2; \quad (\ell \neq j), \tag{A.32}$$

where the denominators for the eight configurations are:

$$\begin{aligned}
\Pi_1 &= \mu_\ell \mu_j - t_{12}^2, \quad \Pi_2 = (\mu_\ell - U_{\ell,j})(\mu_j - U_j) - t_{12}^2, \\
\Pi_3 &= (\mu_\ell - U_{\ell,j})(\mu_j - U_{j,\ell}) - t_{12}^2, \\
\Pi_4 &= (\mu_\ell - 2U_{\ell,j})(\mu_j - U_j - U_{j,\ell}) - t_{12}^2, \\
\Pi_5 &= (\mu_\ell - U_\ell)(\mu_j - U_{j,\ell}) - t_{12}^2, \\
\Pi_6 &= (\mu_\ell - U_\ell - U_{\ell,j})(\mu_j - U_j - U_{j,\ell}) - t_{12}^2,
\end{aligned}$$

$$\begin{aligned}
\Pi_7 &= (\mu_\ell - U_\ell - U_{\ell,j})(\mu_j - 2U_{j,\ell}) - t_{12}^2, \\
\Pi_8 &= (\mu_\ell - U_\ell - 2U_{\ell,j})(\mu_j - U_j - 2U_{j,\ell}) - t_{12}^2.
\end{aligned}$$

We emphasize that the current formula of Eq. (A.30) is correct up to the second order in t_{12} . Taking into account those off-diagonal expectation values such as $\langle n_{12\sigma} \rangle$ can give a more accurate current formula. However, in the limit of our interest where t_{12} is much smaller than the other energy scales, we do not expect any **major** difference.

In this equation-of-motion framework, the expectation values $\langle n_{\ell,\sigma} \rangle$ and c_ℓ can be readily computed via $\langle n_{\ell,\sigma} \rangle = \int d\epsilon G_{\ell,\ell}^{<} / 2\pi$ and $c_\ell = \int d\epsilon G_{\ell,\ell}^{2,<} / 2\pi$. Now the thermally averaged occupation number is given by

$$\begin{aligned}
N_{\ell,\sigma} &= \langle n_{\ell,\sigma} \rangle = \int \frac{d\epsilon}{2\pi} G_{\ell,\ell}^{<}(\epsilon) \\
&\simeq - \int \frac{d\epsilon}{\pi} f_\ell(\epsilon) \text{Im} G_{\ell,\ell}^r(\epsilon); \quad (t_{12} \ll \Gamma_\ell), \tag{A.33}
\end{aligned}$$

$$\begin{aligned}
c_\ell &= \int \frac{d\epsilon}{2\pi} G_{\ell,\ell}^{2,<}(\epsilon) \\
&\simeq - \int \frac{d\epsilon}{\pi} f_\ell(\epsilon) \text{Im} G_{\ell,\ell}^{2,r}(\epsilon); \quad (t_{12} \ll \Gamma_\ell). \tag{A.34}
\end{aligned}$$

Finally, we compare our results with those in Ref. 17, where Yuan *et al* found the current formula in the small t_{12} limit to be

$$J = \frac{2e}{h} \int d\epsilon t_{12}^2 \text{Im} G_{1,1}^r(\epsilon) \text{Im} G_{2,2}^r(\epsilon) [f_L(\epsilon) - f_R(\epsilon)]. \tag{A.35}$$

From this current expression we understand that the density of states for the SCQD is determined by the product of the density of states of each QD, as expected in the small t_{12} limit. Their solution for the retarded **GF** is

$$\begin{aligned}
G_{\ell,\ell}^r(\epsilon) &= \frac{1}{\frac{(\epsilon - E_{\ell,\sigma})(\epsilon - E_{\ell,\sigma} - U_\ell)}{\epsilon - E_\ell - U_\ell(1 - N_{\ell,-\sigma})} + i\Gamma_\ell/2} \\
&\simeq \frac{1 - N_{\ell,-\sigma}}{\epsilon - E_{\ell,\sigma} + i\Gamma_\ell/2} + \frac{N_{\ell,-\sigma}}{\epsilon - E_{\ell,\sigma} - U_\ell + i\Gamma_\ell/2}.
\end{aligned}$$

for $U_\ell \gg \Gamma_\ell$. It can be readily checked that our result is identical to Yuan *et al*'s work if we turn off interdot Coulomb interactions.

† E-mail address: mtkuo@ee.ncu.edu.tw

* E-mail address: yiachang@gate.sinica.edu.tw

-
- ¹ H. Haug and A. P. Jauho, *Quantum Kinetics in Transport and Optics of Semiconductors* (Springer, Heidelberg, 1996).
- ² K. Ono, D. G. Austing, Y. Tokura and S. Tarucha, *science* **297**, 1313 (2002).
- ³ K. Ono and S. Tarucha, *Phys. Rev. Lett.* **92**, 256803 (2004).
- ⁴ A. C. Johnson, J. R. Petta, C. M. Marcus, M. P. Hanson, and A. C. Gossard, *Phys. Rev. B* **72**, 165308 (2005).
- ⁵ N. C. van der Varrt, S.F. Godijn, Y. V. Nazarov, C. J. P. M. Harmans, J. E. Mooij, L. W. Molenkamp, C. T. Foxon, *Phys. Rev. Lett.* **74**, 4702 (1995).
- ⁶ W. G. v. Wiel, S. D. Franceschi, J. M. Elzerman, T. Fujisawa, S. Tarucha, and L. Kouwenhoven, *Rev. Mod. Phys.* **75**, 1 (2003).
- ⁷ Y. Meir and N. S. Wingreen, *Phys. Rev. Lett.* **68**, 2512 (1992).
- ⁸ B. R. Bulka and T. Kostyrko, *Phys. Rev. B* **70**, 205333 (2004).
- ⁹ P. Pals and A. Mackinnon, *J. Phys.: Condens. Matter* **8**, 5401 (1996).
- ¹⁰ S. A. Gurvitz and Y. S. Prager, *Phys. Rev. B* **53**, 15932 (1996).
- ¹¹ J. Fransson, and M. Rasander, *Phys. Rev. B* **73**, 205333 (2006).
- ¹² B. Muralidharan and S. Datta, *Phys. Rev. B* **76**, 035432 (2007).
- ¹³ J. Inarrea, G. Platero, A. H. MacDonald, *Phys. Rev. B* **76**, 085329 (2007).
- ¹⁴ Q. F. Sun, Y. X. Xing, and S. Q. Shen, *Phys. Rev. B* **77**, 195313 (2008).
- ¹⁵ R. Hornberger, S. Koller, G. Begemann, A. Donarini, and M. Grifoni, *Phys. Rev. B* **77**, 245313 (2008).
- ¹⁶ P. Trocha, I. Weymann, and J. Barnas, *Phys. Rev. B* **80**, 165333 (2009).
- ¹⁷ R. Y. Yuan, R. Z. Wang and H. Yan, *J. Phys. Condens. Matter* **19**, 376215 (2007).
- ¹⁸ W. Gong, Y. Zheng, Y. Liu, and T. Lu, *Phys. Rev. B* **73**, 245329 (2006).
- ¹⁹ D. M. T. Kuo, S. Y. Shiau, and Y. C. Chang, arXiv:1101.5751.
- ²⁰ A. Vidan, R. M. Westervelt, M. Stopa, M. Hanson, and A. C. Gossard, *Appl. Phys. Lett.* **85**, 3602 (2004).
- ²¹ D. Culcer, L. Cywinski, Q. Z Li, X. D. Hu, and S. Das Sarma, *Phys. Rev. B*, **82**, 155312 (2010).
- ²² S. Das Sarma, X. Wang, and S. Yang, *Phys. Rev. B*, **83**, 235314 (2011).
- ²³ P. Murphy, S. Mukerjee, J. Morre, *Phys. Rev. B* **78**, 161406 (R) (2008).
- ²⁴ D. M. T. Kuo and Y. C. Chang, *Phys. Rev. B* **81**, 205321 (2010).
- ²⁵ Y. Dubi, and M. Di Ventra, *Rev Modern Phys* **83**, 131 (2011).
- ²⁶ X. Zianni, *Phys. Rev. B* **78**, 165327 (2008).
- ²⁷ R. Sanchez and M. Buttiker, *Phys. Rev. B* **83**, 085428 (2011).
- ²⁸ D. M. T. Kuo and Y. C. Chang, *Phys. Rev. Lett.* **99**, 086803 (2007); Y. C. Chang and D. M. T. Kuo, *Phys. Rev. B* **77**, 245412 (2008).
- ²⁹ B. Dong, H. L. Cui, and X. L. Lei, *Phys. Rev. B* **69**, 035324 (2004).
- ³⁰ B. Wunsch, M. Braun, J. Konig, and D. Pfannkuche, *Phys. Rev. B* **72**, 205319 (2005).
- ³¹ L. Djuric, B. Dong, and H. L. Cui, *J. Appl. Phys.* **99**, 063710 (2006).
- ³² J. Aghassi, A. Thielmann, M. H. Hettler, and G. Schon, *Phys. Rev. B* **73**, 195323 (2006).
- ³³ J. N. Pederson, B. Lassen, A. Wacker, and M. H. Hettler, *Phys. Rev. B* **75**, 235314 (2007).
- ³⁴ D. S. Saraga and D. Loss, *Phys. Rev. Lett.* **90**, 166803 (2003).
- ³⁵ L. Oroszlany, A. Kormayous, J. Koltai, J. Cserti, and C. J. Lambert, *Phys. Rev. B* **76**, 045318 (2007).
- ³⁶ C. Niu, D. L. Lin, and T. H. Lin, *J. Phys. Condens. Matter* **11**, 1511(1999).

Figure Captions

Fig. 1. Tunneling current as a function of applied bias for the variation of U_{12} at temperature $k_B T = 1\Gamma_0$, and $\Gamma_L = \Gamma_R = 0.5\Gamma$. $E_1 = E_F - 10\Gamma_0$ and $E_2 = E_F - 30\Gamma_0$. $J_0 = 2 \times 10^{-3} e\Gamma_0/h$. Other physical parameters $\Gamma_L = \Gamma_R = 0.5\Gamma_0$, and $t_{12} = 0.1\Gamma_0$.

Fig. 2. Tunneling current as a function of applied bias for different temperatures. (a) $E_1 = E_2 = E_F - 10\Gamma_0$ (space symmetrical case), and (b) $E_1 = E_F - 10\Gamma_0$ and $E_2 = E_F - 30\Gamma_0$ (space symmetry breaking). Other physical parameters are the same as the black line of Fig. 1.

Fig. 3. Tunneling current as a function of applied bias at $k_B T = 1\Gamma_0$ in the absence of inter-SCQD electron Coulomb interactions. $t_{12} = t_{34} = 0.025\Gamma_0$ and $t_{14} = t_{32} = 0.01\Gamma_0$. $\Gamma_L = \Gamma_R = 0.5\Gamma_0$. $E_\ell = E_F - 10\Gamma_0$, $U_\ell = 30\Gamma_0$. and $U_{12} = U_{34} = 10\Gamma_0$.

Fig. 4. Tunneling current as a function of applied bias at $k_B T = 1\Gamma_0$ in the absence of inter-SCQD electron Coulomb interactions. $E_1 = E_3 = E_F - 10\Gamma_0$, and $E_2 = E_4 = E_F - 30\Gamma_0$. Other physical parameters are the same as Fig. 3.

Fig. 5. Tunneling current as a function of applied bias at $k_B T = 1\Gamma_0$ in the presence of inter-SCQD electron Coulomb interactions. $U_{14} = U_{32} = 3\Gamma_0$ and $U_{13} =$

$U_{24} = 5\Gamma_0$ Other physical parameters are the same as Fig. 4.

Fig. 6. Tunneling current as a function of applied bias for different energy levels of E_3 at $E_4 = E_F + 10\Gamma_0$ and $k_B T = 1\Gamma_0$ for the SCQD with two energy levels per dot (E_1 and E_3 in dot 1 and E_2 and E_4 in dot 2). Other physical parameters are the same as Fig. 5.

Fig. 7. (a) Electrical conductance G_e and (b) Seebeck coefficient S of the SCQD with $E_1 = E_F - 10\Gamma_0$ and $E_2 = E_F + 20\Gamma_0 - eV_g$ as functions of gate voltage for various temperatures. Other physical parameters are the same as the black line of Fig. 1.

Fig. 8. The electrical conductance G_e and Seebeck coefficient S as a function of gate voltage for different temperatures at $E_1 = E_2 = E_0 = E_F + 20\Gamma_0 - eV_g$. Other physical parameters are the same as the black line of Fig. 1.

Fig. 9. The electrical conductance G_e and Seebeck coefficient S as a function of temperature for the spin triplet states (dashed lines) and spin singlet state (solid lines). For dashed lines, the SCQD is spatially symmetric (triplet state) with $E_1 = E_2 = E_F - 10\Gamma_0$. For solid lines the SCQD is spatially asymmetric (singlet state) with $E_1 = E_F - 10\Gamma_0$ and $E_2 = E_F - 30\Gamma_0$. Here $U_{12} = 10\Gamma_0$.

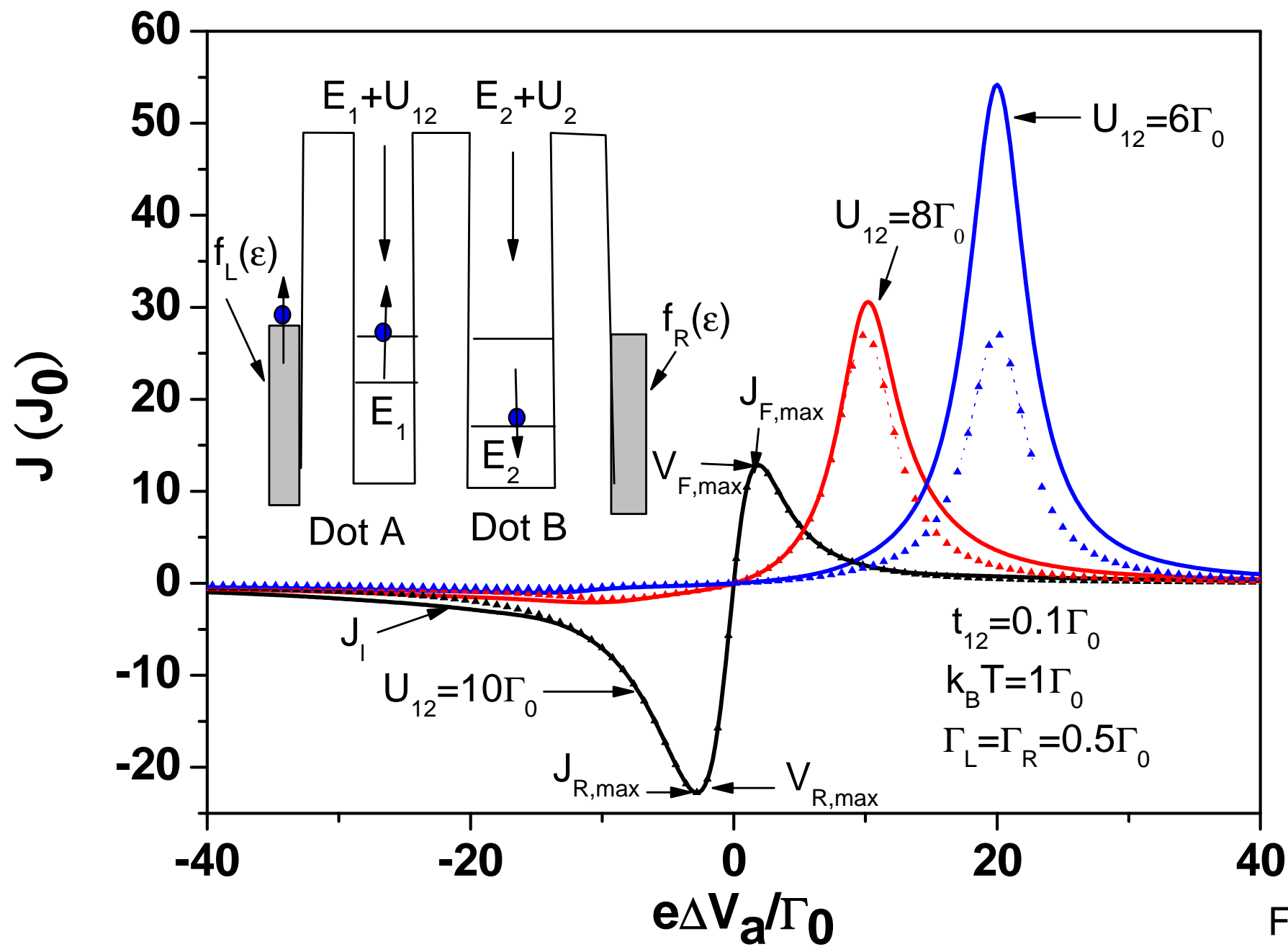


Fig1

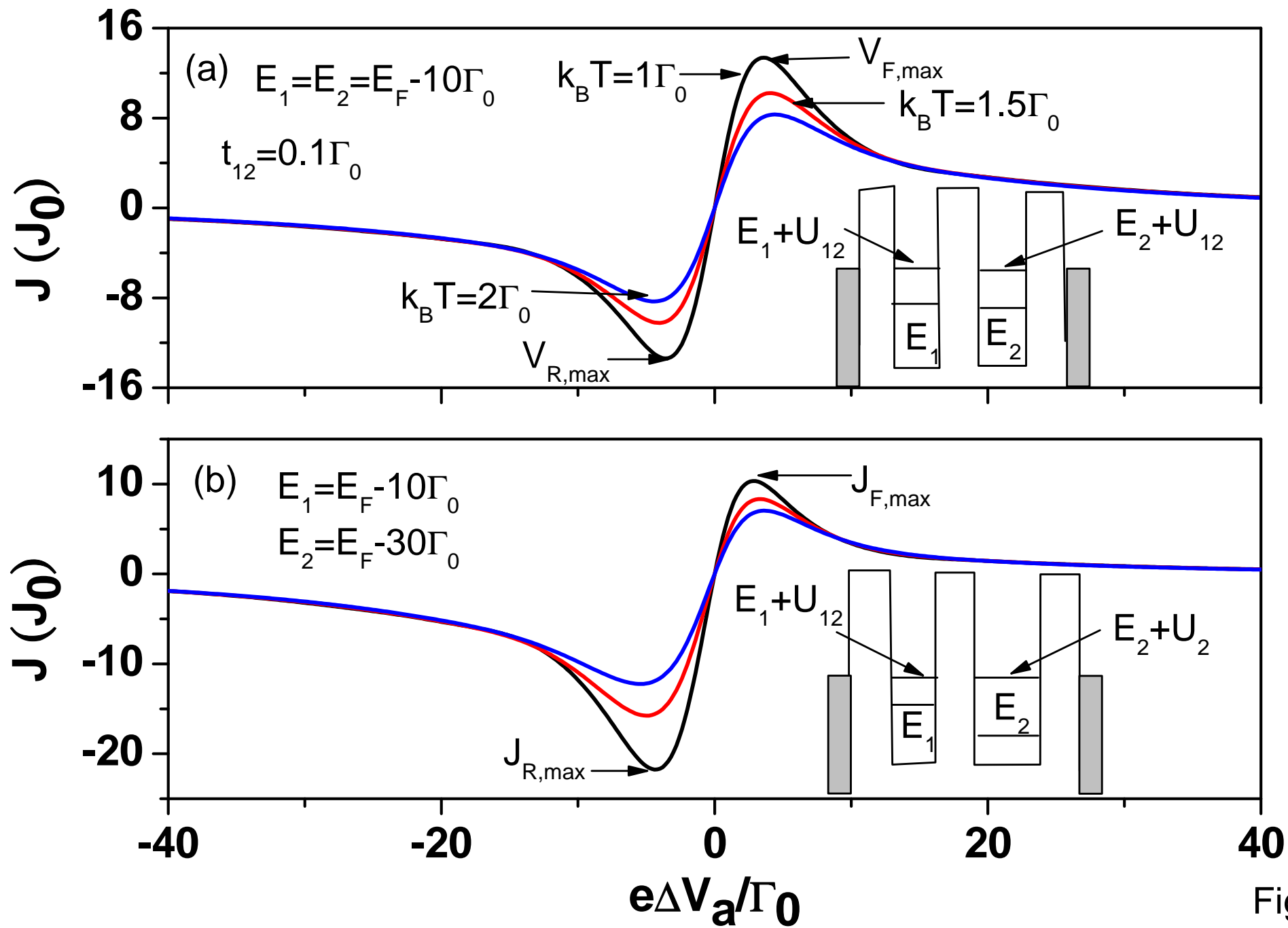


Fig2

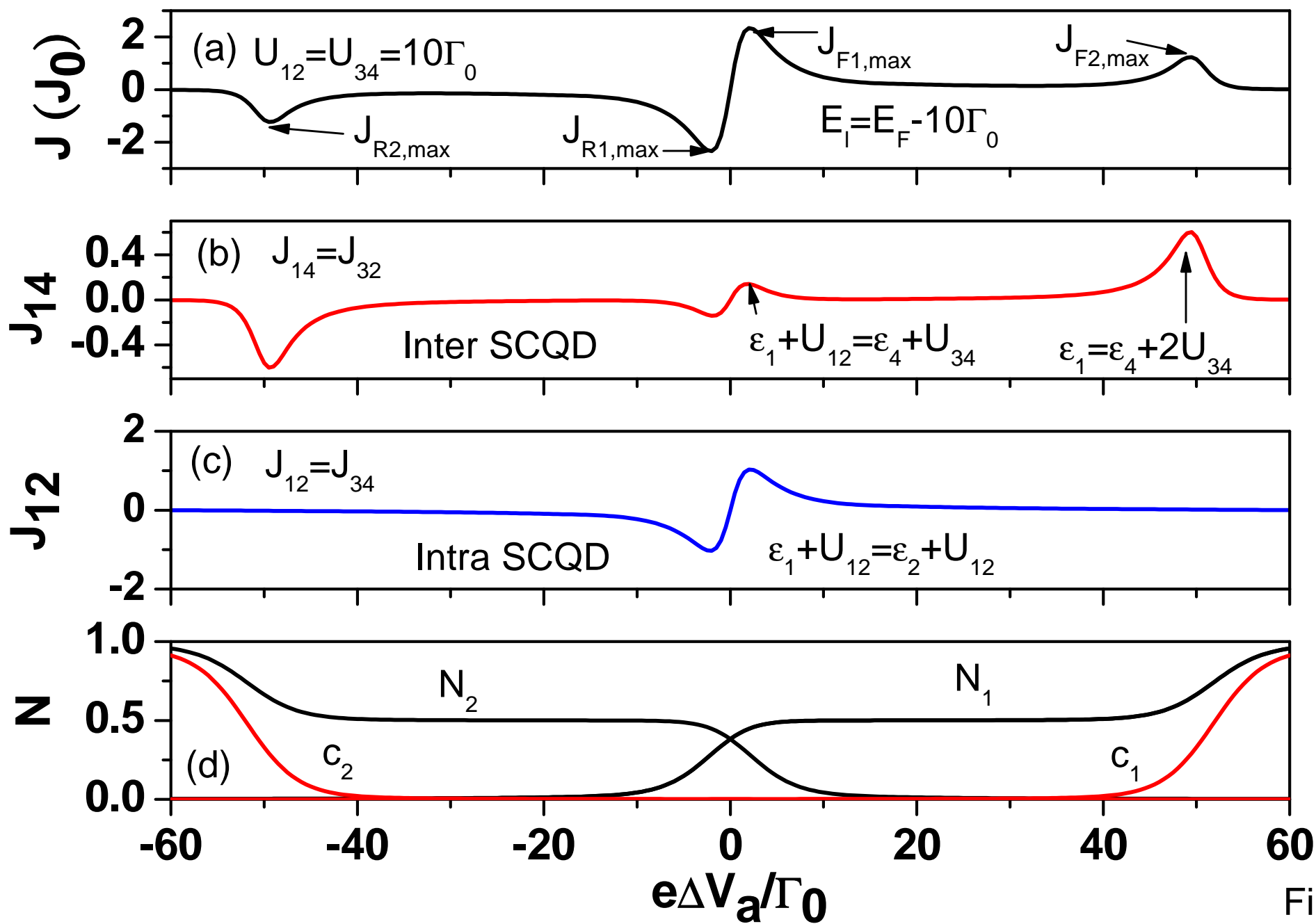


Fig3

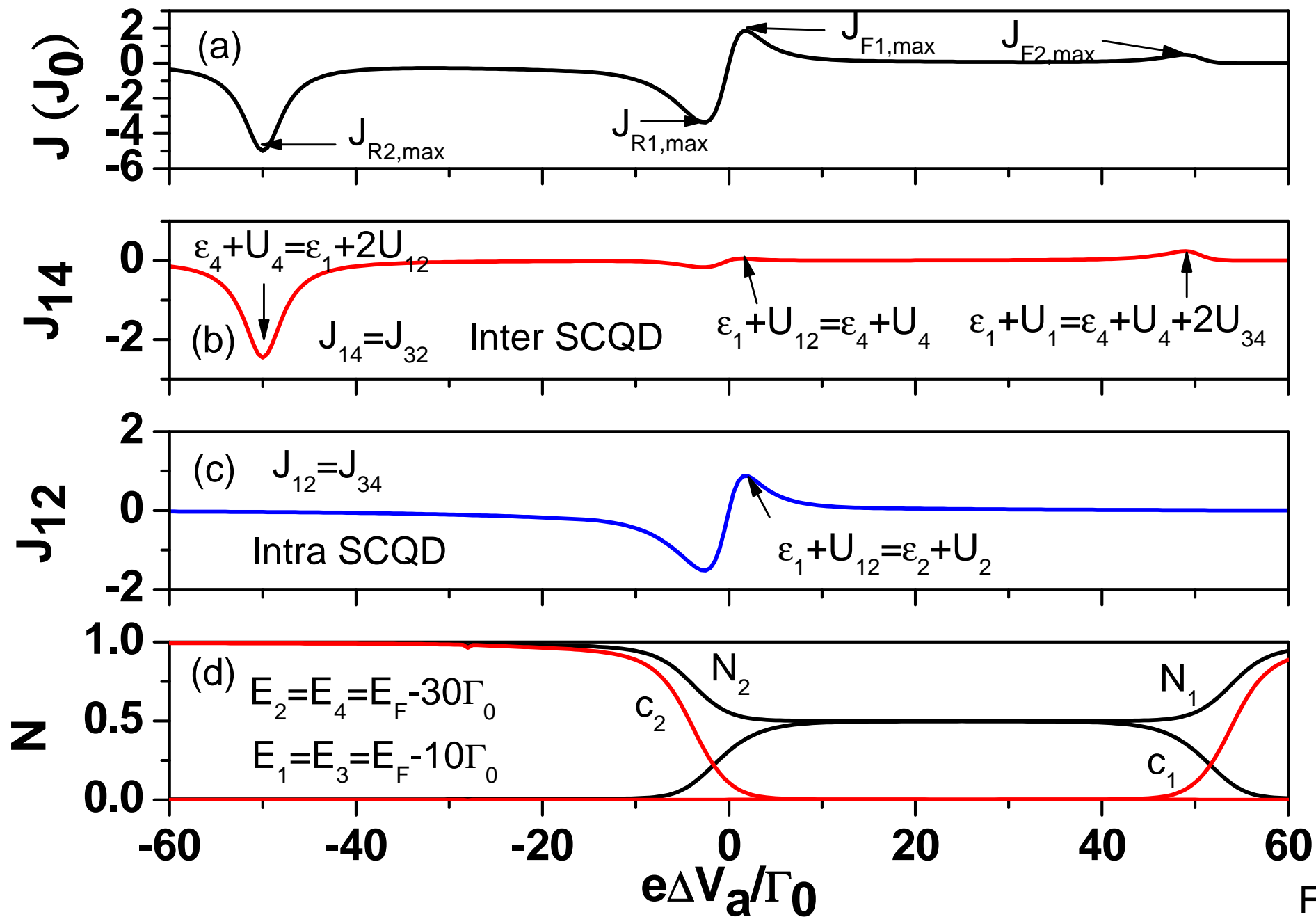


Fig4

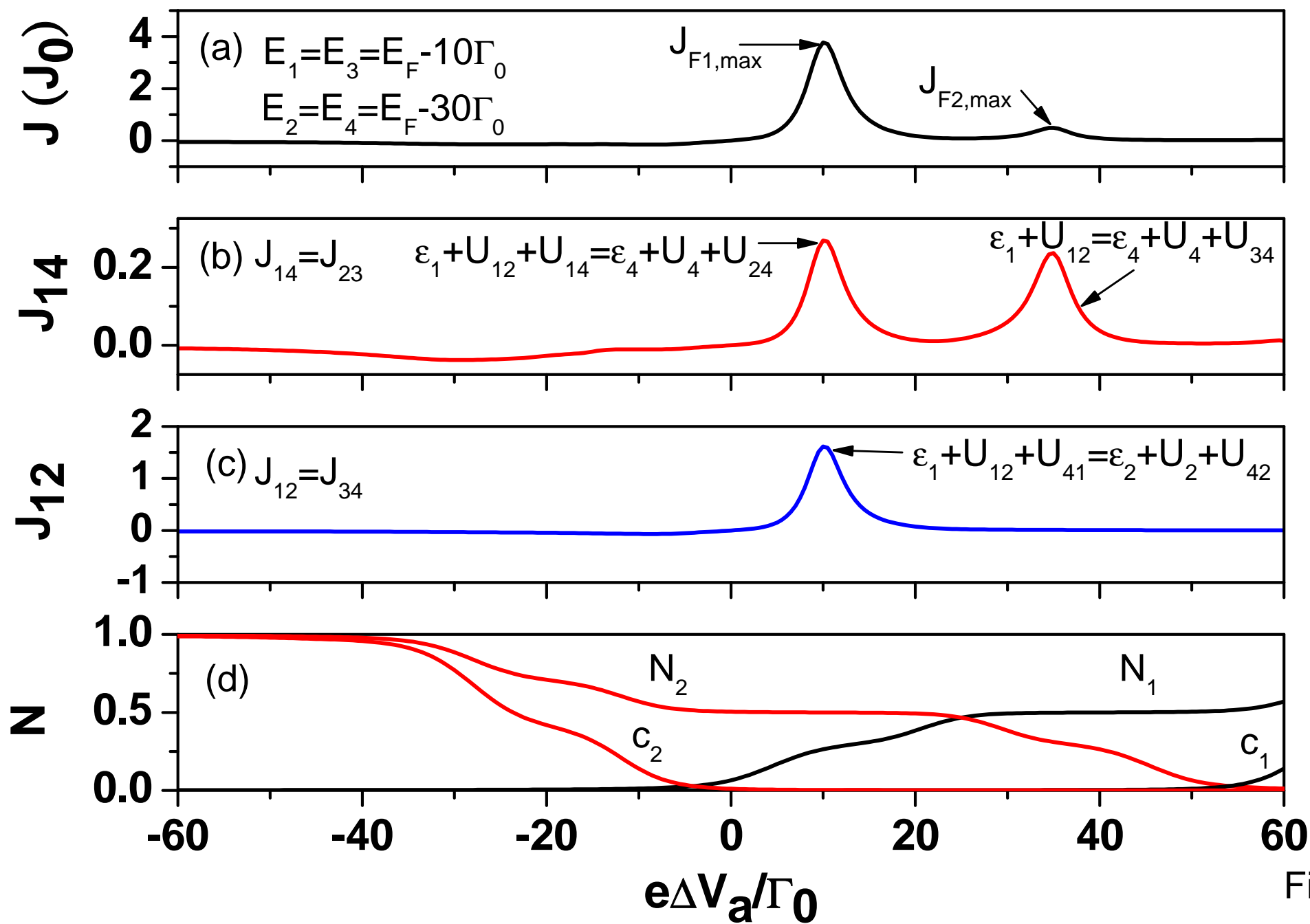


Fig5

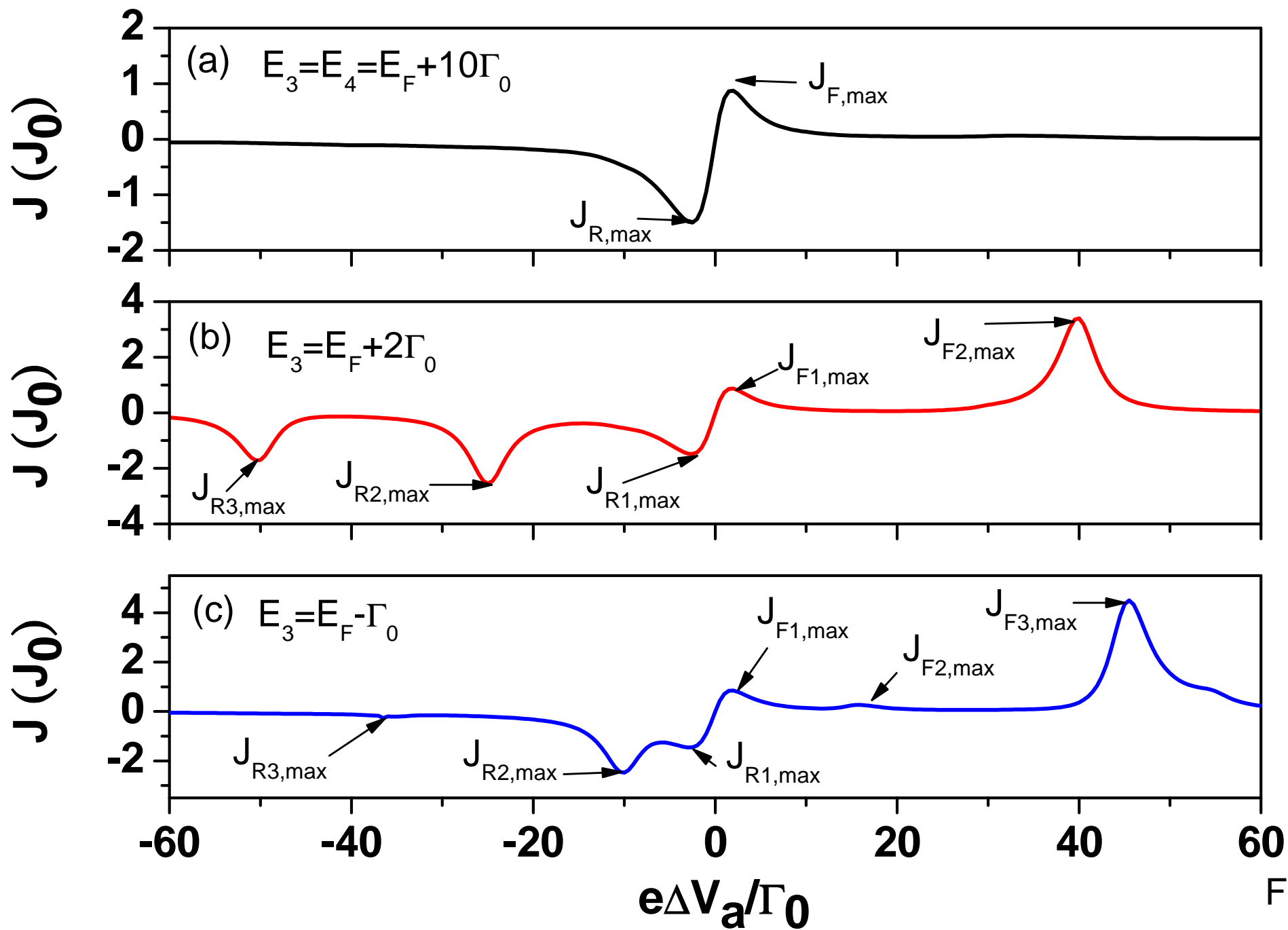


Fig6

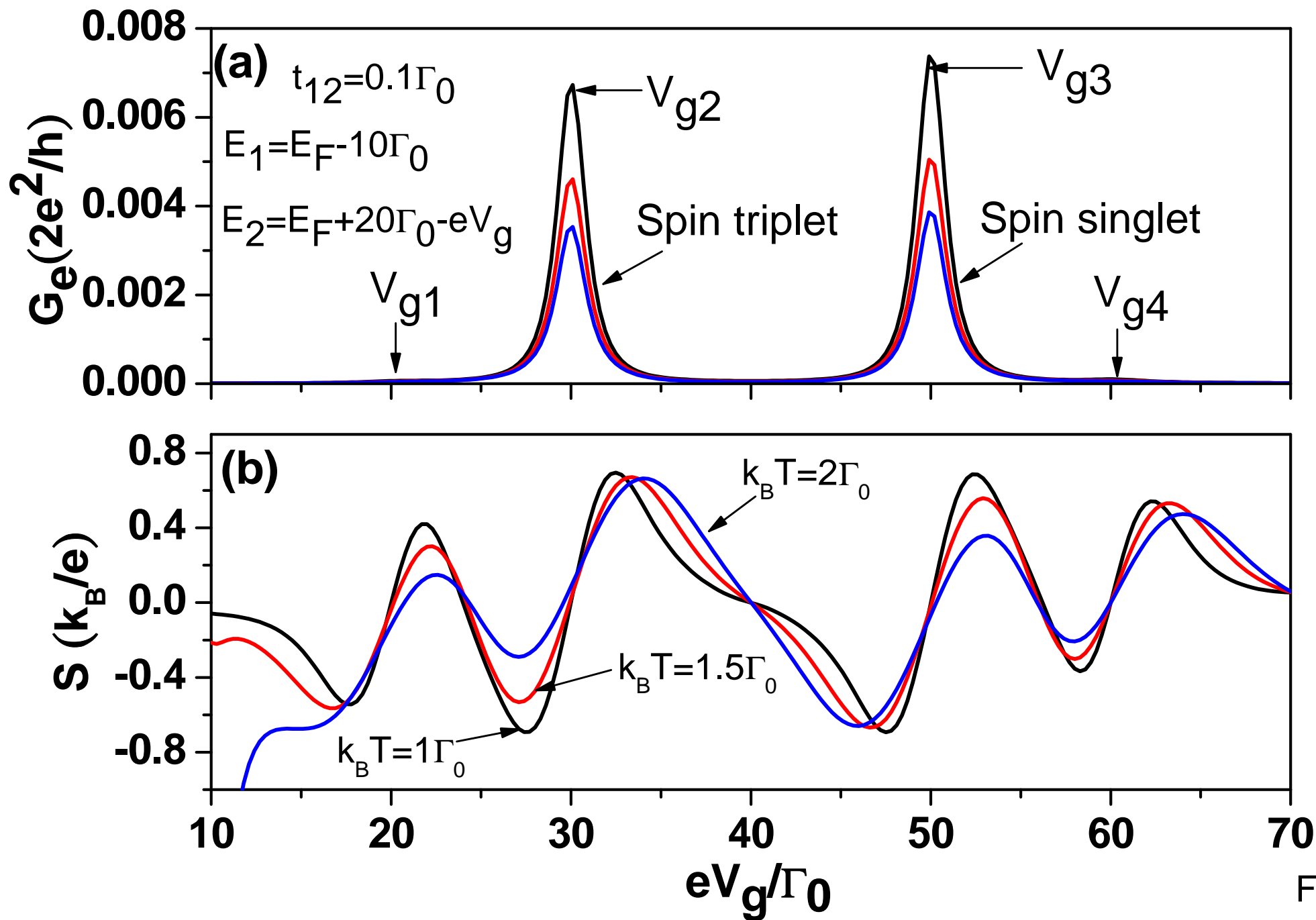


Fig7

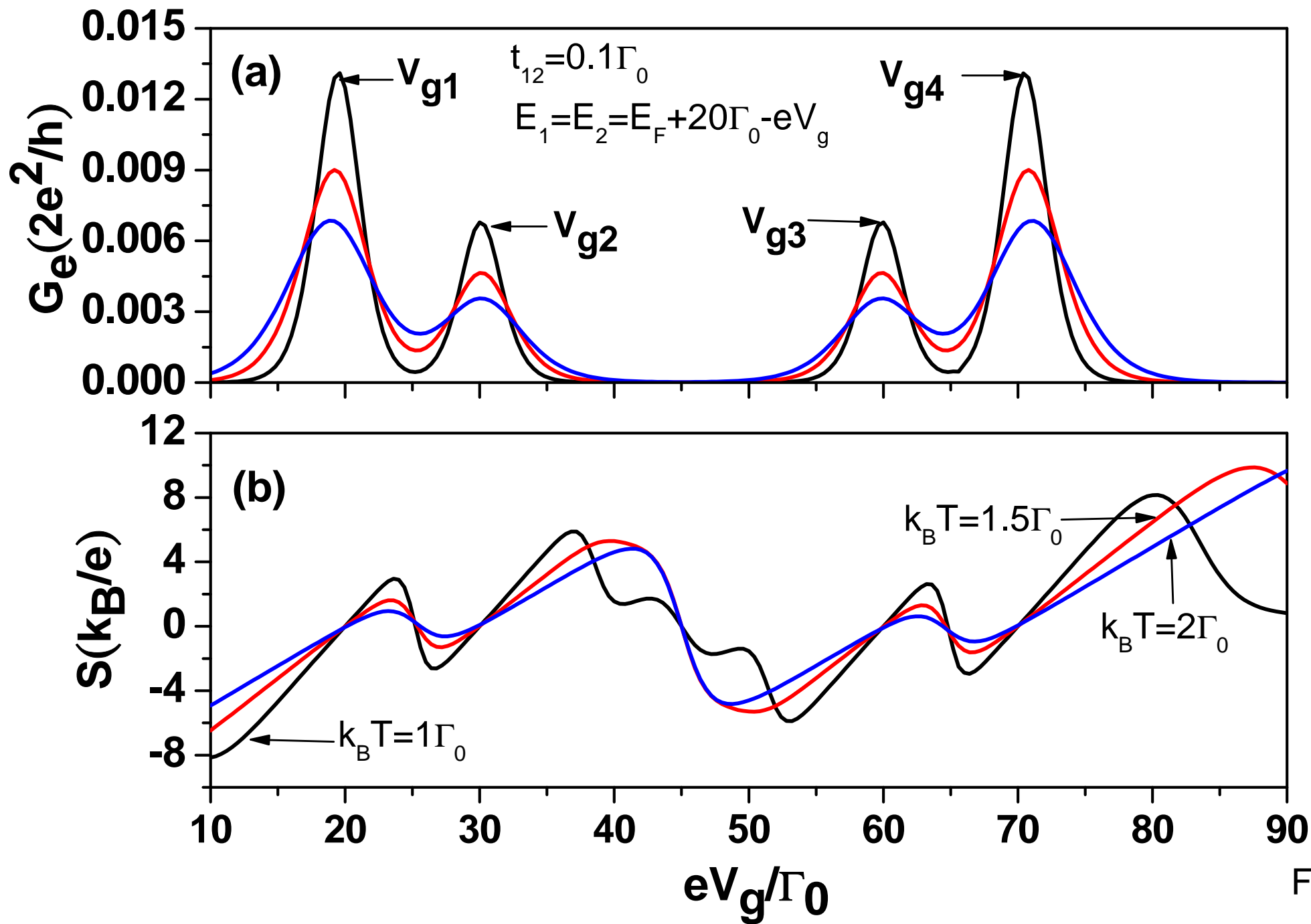


Fig8

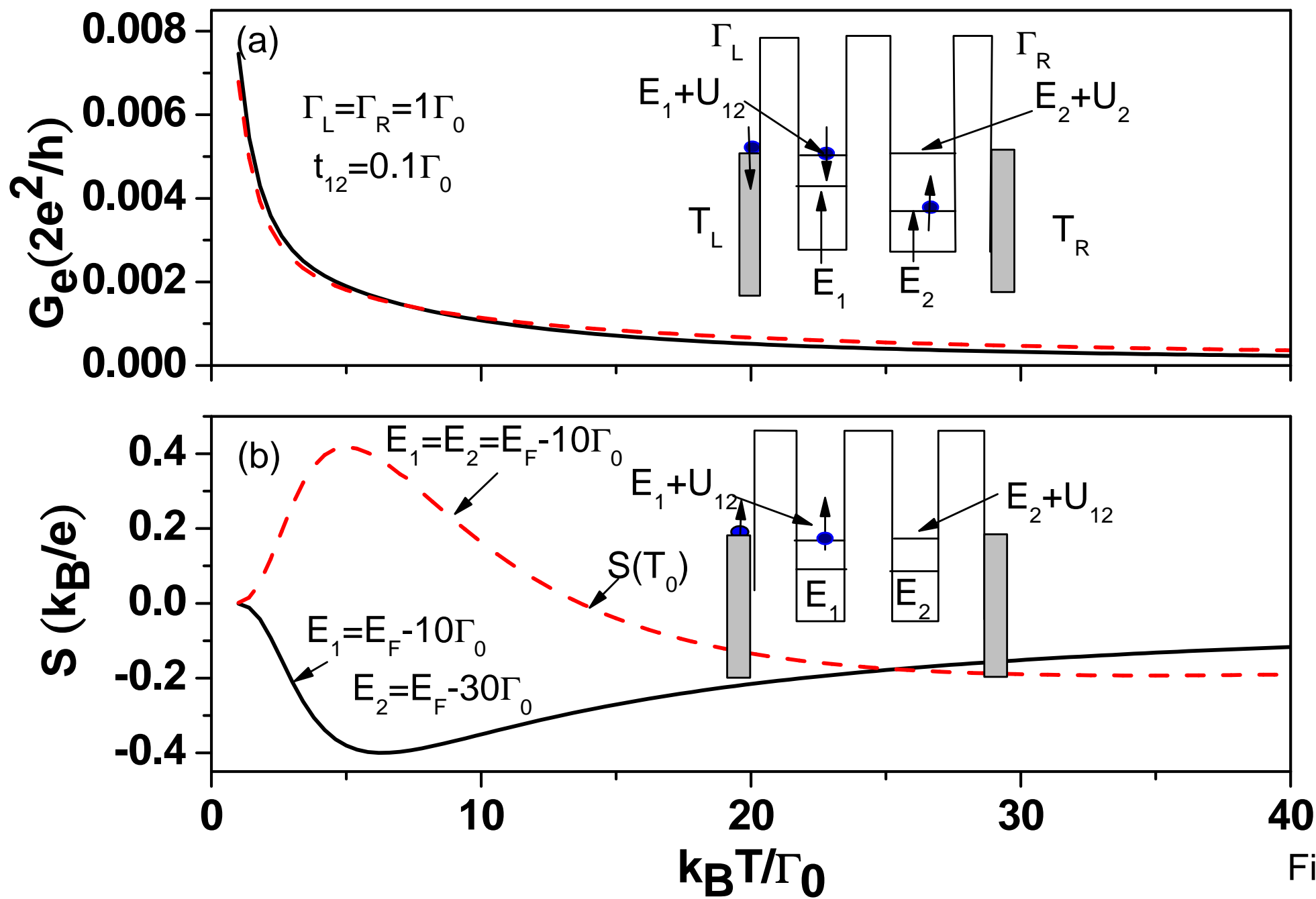


Fig9